

# Distributionally robust risk evaluation with causality constraint and structural information

Bingyan Han <sup>\*</sup>

March 22, 2022

## Abstract

This work studies distributionally robust evaluation of expected function values over temporal data. A set of alternative measures is characterized by the causal optimal transport. We prove the strong duality and recast the causality constraint as minimization over an infinite-dimensional test function space. We approximate test functions by neural networks and prove the sample complexity with Rademacher complexity. Moreover, when structural information is available to further restrict the ambiguity set, we prove the dual formulation and provide efficient optimization methods. Simulation on stochastic volatility and empirical analysis on stock indices demonstrate that our framework offers an attractive alternative to the classic optimal transport formulation.

**Keywords:** Risk management, distributionally robustness, causal optimal transport, stochastic volatility, minimax optimization, Rademacher complexity.

## 1 Introduction

The measurement of risk or other objectives relies on the choice of the underlying probability measure. The decision-maker (DM) faces a challenge to imposing an expressive but tractable reference measure. One simple choice is the empirical measure on a sample data set. However, since the sample size may be small and/or the observations are blurred by noises, the assumed reference measure is prone to model misspecification. Moreover, time-series data are fundamental and essential in many areas. The temporal structure poses another difficulty to modeling and thus another source of misspecification. The main goal of this paper is to provide a robust framework for risk evaluation with temporal data.

Since Knight (1921) clarified the subtle difference between risk and model uncertainty (misspecification), there have been several methodologies to incorporate robustness. Commonly, the objective is evaluated over a set of alternative plausible measures instead. Hansen and Sargent (2001) pioneered the robust control paradigm when alternative measures are equivalent to the reference measure and relative entropy quantifies the distinction between two measures. Along this direction, Uppal and Wang (2003); Maenhout (2004); Ben-Tal et al. (2010); Han et al. (2021) investigated robust optimization in portfolio selection and asset pricing problems; see Hansen (2014) for a review on model uncertainty. One limitation of relative entropy, however, is that it cannot compare non-equivalent measures when ambiguous volatility appears. Nonlinear expectations (Peng, 2010) and McKean-Vlasov dynamic programming (Ismail and Pham, 2019) are two approaches to tackle the volatility uncertainty. The third paradigm utilizes Wasserstein

---

<sup>\*</sup>Email: hanbyan@gmail.com. Homepage: <https://sites.google.com/site/hanbyan/>

distance and optimal transport (Villani, 2009). Wasserstein distance is the minimum cost incurred by an optimal coupling, also known as an optimal transport plan, that can reshape the reference measure to the alternative measure, probably with different supports.

Optimal transport (OT) enjoys intuitive geometric interpretation and has found interdisciplinary applications in mathematics, machine learning, statistics, and economics; see Villani (2009); Santambrogio (2015); Galichon (2016); Peyré et al. (2019) for a book-level introduction. One can embed flexible structures into the cost function of OT. Besides the modeling flexibility, OT also demonstrates great analytical tractability and can be solved in explicit forms or with efficient algorithms. Applications of OT in model uncertainty dated at least back to Pflug and Wozabal (2007), in which the ambiguity set is defined by the Wasserstein distance of order one. Gao and Kleywegt (2016) considered distributionally robust stochastic optimization (DRSO) with ambiguity sets characterized by the Wasserstein distance of order  $p$ . Mohajerin Esfahani and Kuhn (2018) proved that some DRSO problems have a finite convex program formulation. Blanchet and Murthy (2019) allowed general lower semi-continuous cost functions and proved strong duality results with general Polish spaces as domains. Guo and Obłój (2019); Zhou et al. (2021) and reference therein investigated martingale optimal transport with problems from option pricing and hedging. Applications in risk management and portfolio selection are considered by Bartl et al. (2020); Eckstein et al. (2020); Blanchet et al. (2021).

However, OT needs a proper formulation to acknowledge the chronological structure in temporal data. Several researchers have introduced seemly different adapted versions of Wasserstein distance. Lassalle (2013) imposed a causality constraint on the transport plans between discrete stochastic processes and termed it as causal optimal transport (COT). Pflug and Pichler (2012) defined a notion of *nested distance*, which can be roughly regarded as bicausal. A recent work of Backhoff-Veraguas et al. (2020b) proved these definitions and many others define the same topology in finite discrete time. Roughly speaking, given the past of a process  $X$ , the past of another process  $Y$  should be independent of the future of  $X$  under the transport plan measure. As a rising area, COT has found applications in mathematical finance (Backhoff-Veraguas et al., 2020a), video modeling (Xu et al., 2020; Xu and Acciaio, 2021), mean-field games (Acciaio et al., 2021), and stochastic optimization (Pflug and Pichler, 2012; Acciaio et al., 2020). In this paper, we study risk evaluation with temporal data and ambiguity sets characterized by COT.

Our contributions are from both theoretical and practical perspectives. We first prove the strong duality theorem with lower semi-continuous costs. Compared with OT paradigm in Gao and Kleywegt (2016); Blanchet and Murthy (2019), the causality constraint adds an extra infinite-dimensional optimization problem. Motivated by the scalability and the universal approximation property of neural networks, we use them to approximate the infinite-dimensional test function space. We further prove the sample complexity results with the classic Rademacher complexity theory. Before considering general empirical experiments, we use one analytical example to show the essential difference between OT and COT. In the extreme case, OT can completely ignore the non-anticipativeness and yield distinct solutions compared with COT. However, when the cost and the objective are separable, we prove that OT and COT obtain the same worst-case scenarios. More importantly, a special example with a linear objective and quadratic cost reveals some undesired properties of OT and COT. The worst-case scenario merely shifts the sample paths of the empirical distributions by a constant depending on the radius of the Wasserstein ball. The worst-case paths rely on the reference samples *pathwisely and pointwisely*; see Figure (2a) later for an example. Moreover, the temporal structure in the worst-case is the same as the reference one. It absorbs any potential noises in the empirical distributions. These observations reveal that OT and COT may contain unrealistic alternative scenarios and can be conservative.

To further rule out some unrealistic scenarios in the Wasserstein ball, we propose a new framework to embed structural beliefs of the DM into alternative measures and term it as structural COT (SCOT). The duality theorem links the SCOT primal problem with calculations

of the Wasserstein distance under modified costs. We prove a finite sample guarantee result for SCOT and COT. The structural information rules out conservative paths and finds the worst scenarios different from the reference data. Unfortunately, there is no universal rule on embedding structural information since it is usually problem-specific. Thus, we provide two numerical examples to demonstrate the essential idea. The first example is volatility estimation, where the DM is concerned about the average volatility levels over a certain period. The alternative model is a Jacobi model (Ackerer et al., 2018) with unknown parameters. The long-term mean level parameter is decomposed into reference sample averages and an extra learnable parameter. We find that SCOT can acknowledge the temporal structure and generate more meaningful alternative scenarios. The second example is the prediction of the S&P 500 index. The design of the alternative model is inspired by the residual networks (He et al., 2016). We perturb the original data by random noises and outputs of neural networks, aiming to generate worst-case scenarios that lead to upper bounds of future S&P 500 index levels. Empirically, our SCOT method achieves a better trade-off between prediction accuracy and mean absolute errors in the out-of-sample testing.

The rest of the paper is organized as follows. Section 2 introduces the backgrounds and formulates the primal problem of interest. Section 3 proves the strong duality of COT formulation and motivates the SCOT framework. Section 4 proves the sample complexity results and gives the optimization algorithms. Section 5 presents the numerical analysis and compares different methodologies. Section 6 concludes the paper with further directions. Training details are in the Appendix.

## 2 Problem formulation

Let integer  $T$  be the finite number of periods. Denote  $[T] := \{1, 2, \dots, T-1, T\}$ . For each  $t \in [T]$ , suppose  $\Omega_t$  is a closed (but not necessarily bounded) subset of  $\mathbb{R}$ .  $\Omega_t$  is interpreted as the range of the process at time  $t$ . We consider a one-dimensional process merely for the ease of presentation. Our results can be extended to multi-dimensional processes directly.  $\Omega_{1:T} := \Omega_1 \times \dots \times \Omega_T$  is a closed subset of  $\mathbb{R}^T$ . We also use a notation  $\mathcal{X} := \Omega_{1:T}$  to distinguish the reference measure from alternative measures. Let  $C_b(\Omega_{1:t})$  be the set of all continuous and bounded functions on  $\Omega_{1:t}$  and  $\mathcal{P}(\mathcal{X})$  be the set of all Borel probability measures on  $\mathcal{X}$ . The decision-maker (DM) observes data from the underlying true but unknown probability measure  $\mu \in \mathcal{P}(\mathcal{X})$ . Then the DM constructs the reference measure  $\hat{\mu}$  and a typical example is the empirical measure.

With the reference measure  $\hat{\mu}$ , a fundamental problem is to evaluate the expectation

$$\int_{\mathcal{X}} f(x) \hat{\mu}(dx) \tag{2.1}$$

for some given function  $f$  with technical assumptions specified later. Examples in finance include value-at-risk (VaR) and volatility estimation, to name a few. Following the convention in Blanchet and Murthy (2019); Gao and Kleywegt (2016), we refer to the problem (2.1) as risk evaluation.

An essential difficulty in risk evaluation is the reference measure  $\hat{\mu}$  can be misspecified. Commonly, it is difficult or even impossible to obtain a sufficiently large data set. Besides, observations may exhibit a high level of noise, especially in financial data. To incorporate robustness into risk evaluation, an approach is to consider some close but different measures as alternatives to  $\hat{\mu}$ . A methodology is distributionally robust risk evaluation with an optimal transport framework. We review the paradigm as follows.

Consider another probability measure  $\nu \in \mathcal{P}(\mathcal{Y})$  on a domain  $\mathcal{Y}$  as an alternative measure. For simplicity, we suppose  $\mathcal{Y} = \Omega_{1:T}$  is the same as  $\mathcal{X}$ , while in general, they can be distinct. A coupling  $\pi \in \mathcal{P}(\mathcal{X} \times \mathcal{Y})$  is a Borel probability measure that admits  $\hat{\mu}$  and  $\nu$  as its marginals on  $\mathcal{X}$  and  $\mathcal{Y}$ , respectively. Denote  $\Pi(\hat{\mu}, \nu)$  as the set of all the couplings.  $\pi(x, y)$  is usually known

as a transport plan between  $\hat{\mu}$  and  $\nu$ . Heuristically, one can interpret  $\pi(x, y)$  as the probability mass moved from  $x$  to  $y$ .

Suppose transporting one unit of mass from  $x$  to  $y$  incurs a cost of  $c(x, y)$ . The classic optimal transport (OT) problem is formulated as

$$\mathcal{W}(\hat{\mu}, \nu) := \inf_{\pi \in \Pi(\hat{\mu}, \nu)} \int_{\mathcal{X} \times \mathcal{Y}} c(x, y) \pi(dx, dy). \quad (2.2)$$

Intuitively,  $\mathcal{W}(\hat{\mu}, \nu)$  quantifies how difficult it is to reshape the measure  $\hat{\mu}$  to  $\nu$ . Blanchet and Murthy (2019) considers the risk evaluation over alternative measures  $\nu$  in the Wasserstein ball with a radius of  $\varepsilon > 0$ :

$$\sup_{\nu} \int_{\mathcal{Y}} f(y) \nu(dy), \text{ subject to } \mathcal{W}(\hat{\mu}, \nu) \leq \varepsilon. \quad (2.3)$$

We refer to the problem (2.3) as the OT risk evaluation or simply the OT method (formulation).

In this work, we consider the temporal data as  $x = (x_1, \dots, x_t, \dots, x_T)$ , which are common in statistics and finance. Then a natural requirement of the transport plan  $\pi(x, y)$  is the non-anticipative condition. Indeed, if the past of  $x$  is given, then the past of  $y$  should be independent of the future of  $x$  under the measure  $\pi$ . Mathematically, a transport plan  $\pi$  should satisfy

$$\pi(dy_t | dx_{1:T}) = \pi(dy_t | dx_{1:t}), \quad t = 1, \dots, T - 1. \quad (2.4)$$

The property (2.4) is known as the causality condition and the transport plan satisfying (2.4) is called *causal* by Lassalle (2013). Denote  $\Pi_c(\hat{\mu}, \nu)$  as the set of all causal transport plans between  $\hat{\mu}$  and  $\nu$ .

In contrast to the OT formulation (2.2), the causal optimal transport (COT) problem with temporal data restricts to minimize the cost only over  $\Pi_c(\hat{\mu}, \nu)$ :

$$\mathcal{W}_c(\hat{\mu}, \nu) := \inf_{\pi \in \Pi_c(\hat{\mu}, \nu)} \int_{\mathcal{X} \times \mathcal{Y}} c(x, y) \pi(dx, dy). \quad (2.5)$$

Denote the causal Wasserstein ball as

$$\mathcal{B}_\varepsilon := \{\nu : \mathcal{W}_c(\hat{\mu}, \nu) \leq \varepsilon\}.$$

The distributionally robust risk evaluation under COT is

$$J(\varepsilon; \hat{\mu}) := \sup_{\nu \in \mathcal{B}_\varepsilon} \int_{\mathcal{Y}} f(y) \nu(dy). \quad (2.6)$$

Since the causality condition may rule out some transport plans, one can expect that  $\mathcal{W}_c(\hat{\mu}, \nu) \geq \mathcal{W}(\hat{\mu}, \nu)$ . The causal Wasserstein ball may contain fewer alternative measures and discard them due to the causality. We call (2.6) the primal problem of the COT risk evaluation. The primal value may be less than the counterpart of the OT method.

Before we present the solution to the primal problem (2.6), we assume the following technical condition on the reference and true measure throughout the paper, to guarantee the well-posedness of the problem.

**Standing Assumption 2.1.** *The reference measure  $\hat{\mu}$  and the true measure  $\mu$  are successively weakly continuous in the sense of Backhoff-Veraguas et al. (2017, Assumption 2.5).*

The conditions on the cost  $c(x, y)$  and the objective function  $f$  may vary in different results. We impose them later in the subsequent sections.

### 3 Duality

A key observation on the causality condition is that it can be formulated as a linear constraint; see Backhoff-Veraguas et al. (2017, Proposition 2.4). In this section, we prove the strong duality theorem for (2.6) and propose an algorithm for the dual problem based on neural networks.

#### 3.1 Strong duality for COT risk evaluation

**Assumption 3.1.** *The objective  $f : \mathcal{X} \rightarrow \mathbb{R}$  is upper semi-continuous (u.s.c.) and  $\int_{\mathcal{X}} |f(x)|\mu(dx) < \infty$ . The cost  $c(x, y) : \mathcal{X} \times \mathcal{Y} \rightarrow [0, \infty)$  is lower semi-continuous (l.s.c.) and non-negative.*

Compared with Blanchet and Murthy (2019, Assumption 1), we drop the requirement that  $c(x, x) = 0$  but do not allow  $c(x, y)$  to be infinite. It becomes easier to design an analytical example later in Section 3.2 to present differences on several formulations.

Under Assumptions 2.1 and 3.1, Backhoff-Veraguas et al. (2017, Theorem 2.6) proved that the infimum of COT in (2.5) is attained. One can rewrite the primal problem (2.6) as

$$\sup_{\pi} \int_{\mathcal{X} \times \mathcal{Y}} f(y)\pi(dx, dy), \text{ subject to } \pi \in \cup_{\nu} \Pi_c(\hat{\mu}, \nu), \text{ and } \int_{\mathcal{X} \times \mathcal{Y}} c(x, y)\pi(dx, dy) \leq \varepsilon.$$

As preparation for proving the strong duality, we introduce a test function space as

$$\begin{aligned} \Gamma := \Big\{ \gamma : \mathcal{X} \times \mathcal{Y} \rightarrow \mathbb{R} \Big| \gamma(x, y) &= \sum_{l=1}^L \sum_{t=1}^{T-1} h_{l,t}(y_{1:t}) \Big[ g_{l,t}(x_{1:T}) \\ &- \int_{\Omega_{t+1:T}} g_{l,t}(x_{1:t}, x_{t+1:T}) \hat{\mu}(dx_{t+1:T} | x_{1:t}) \Big], \text{ for } h_{l,t} \in C_b(\Omega_{1:t}), g_{l,t} \in C_b(\Omega_{1:T}), \\ &\text{and some positive integer } L \in \mathbb{N} \Big\}. \end{aligned}$$

Theorem 3.2 proves the strong duality for the primal problem (2.6). We assume compact domains to validate Sion's minimax theorem.

**Theorem 3.2.** *Suppose  $\mathcal{X}$  and  $\mathcal{Y}$  are compact, Assumption 3.1 holds, and  $\mathcal{B}_\varepsilon$  is non-empty for certain  $\varepsilon > 0$ , then the strong duality holds as  $J(\varepsilon; \hat{\mu}) = D(\varepsilon; \hat{\mu})$ , where*

$$D(\varepsilon; \hat{\mu}) = \inf_{\lambda \geq 0, \gamma \in \Gamma} \lambda \varepsilon + \int_{\mathcal{X}} F(x; \lambda, \gamma) \hat{\mu}(dx) \quad (3.1)$$

and

$$F(x; \lambda, \gamma) := \sup_{y \in \mathcal{Y}} \{f(y) - \lambda c(x, y) + \gamma(x, y)\}.$$

Moreover, there exists a primal optimizer  $\nu^* \in \mathcal{B}_\varepsilon$  for  $J(\varepsilon; \hat{\mu})$ .

*Proof.* We first prove the claim with continuous  $f(y)$  and  $c(x, y)$ .

Consider  $\pi \in \mathcal{P}(\mathcal{X} \times \mathcal{Y})$  as some Borel probability measure on  $\mathcal{X} \times \mathcal{Y}$ . Constant  $\lambda \geq 0$  serves as the Lagrange multiplier. Note that by Backhoff-Veraguas et al. (2017, Lemma 3.1),

$$g_{l,t}(x_{1:T}) - \int_{\Omega_{t+1:T}} g_{l,t}(x_{1:t}, x_{t+1:T}) \hat{\mu}(dx_{t+1:T} | x_{1:t})$$

is continuous in  $x_{1:T}$  under continuous  $g_{l,t}$  and Assumption 2.1. Then the test function space  $\Gamma \subset C_b(\mathcal{X} \times \mathcal{Y})$ . Moreover,  $\Gamma$  is a convex subset.

Let  $\beta \in C_b(\Omega_{1:T})$ . Introduce the Lagrangian as

$$\begin{aligned}\mathcal{L}(\pi, \lambda, \gamma, \beta) := & \int_{\mathcal{X} \times \mathcal{Y}} (f(y) - \beta(x) + \gamma(x, y)) \pi(dx, dy) + \lambda [\varepsilon - \int_{\mathcal{X} \times \mathcal{Y}} c(x, y) \pi(dx, dy)] \\ & + \int_{\mathcal{X}} \beta(x) \hat{\mu}(dx).\end{aligned}$$

Observing that  $\mathcal{X} \times \mathcal{Y}$  is a compact Polish space, then  $\mathcal{P}(\mathcal{X} \times \mathcal{Y})$  is compact under the weak topology. Since  $f$ ,  $\gamma(x, y)$ , and  $c(x, y)$  are also continuous and the support of  $\pi$  is bounded, we obtain that  $\mathcal{L}$  is continuous in  $\pi$ . Besides, consider the spaces  $C_b(\Omega_{1:T})$  and  $C_b(\mathcal{X} \times \mathcal{Y})$  endowed with uniform topology and  $\lambda \geq 0$  with the Euclidean topology, one has that  $\mathcal{L}$  is continuous in  $\lambda$ ,  $\gamma$ , and  $\beta$ . Moreover,  $\mathcal{L}$  is linear (and thus quasi-concave) in  $\pi$  for given  $(\lambda, \gamma, \beta)$ .  $\mathcal{L}$  is linear (and thus quasi-convex) in  $(\lambda, \gamma, \beta)$  for given  $\pi$ . We have verified that  $\mathcal{L}$  satisfies the conditions of Sion's minimax theorem, which yields

$$\sup_{\pi \in \mathcal{P}(\mathcal{X} \times \mathcal{Y})} \inf_{\substack{\lambda \geq 0, \gamma \in \Gamma, \\ \beta \in C_b(\Omega_{1:T})}} \mathcal{L}(\pi, \lambda, \gamma, \beta) = \inf_{\substack{\lambda \geq 0, \gamma \in \Gamma, \\ \beta \in C_b(\Omega_{1:T})}} \sup_{\pi \in \mathcal{P}(\mathcal{X} \times \mathcal{Y})} \mathcal{L}(\pi, \lambda, \gamma, \beta). \quad (3.2)$$

We validate that the left-hand side (LHS) equals to the primal value  $J(\varepsilon; \hat{\mu})$  and the right-hand side (RHS) reduces to the dual value  $D(\varepsilon; \hat{\mu})$ .

Consider the LHS first. Given some  $\pi \in \mathcal{P}(\mathcal{X} \times \mathcal{Y})$ , if the inner infimum of LHS is not equal to  $-\infty$ , then  $\pi$  must satisfy

$$\begin{aligned}\int_{\mathcal{X} \times \mathcal{Y}} \beta(x) \pi(dx, dy) &= \int_{\mathcal{X}} \beta(x) \hat{\mu}(dx), \\ \int_{\mathcal{X} \times \mathcal{Y}} \sum_{t=1}^{T-1} h_{l,t}(y_{1:t}) [g_{l,t}(x_{1:T}) - \int_{\Omega_{t+1:T}} g_{l,t}(x_{1:t}, x_{t+1:T}) \hat{\mu}(dx_{t+1:T} | x_{1:t})] \pi(dx, dy) &= 0, \quad l \in [L], \\ \int_{\mathcal{X} \times \mathcal{Y}} c(x, y) \pi(dx, dy) &\leq \varepsilon,\end{aligned}$$

for any  $h_{l,t} \in C_b(\Omega_{1:t})$  and  $g_{l,t}, \beta \in C_b(\Omega_{1:T})$ . With compact supports, the first condition implies that the marginal of  $\pi$  on  $\mathcal{X}$  is the reference measure  $\hat{\mu}$ . By Backhoff-Veraguas et al. (2017, Proposition 2.4), the second condition guarantees that  $\pi$  is a causal transport plan on  $\mathcal{X} \times \mathcal{Y}$  between  $\hat{\mu}$  and the marginal of  $\pi$  on  $\mathcal{Y}$ . Together with the third inequality, we conclude that the marginal of  $\pi$  on  $\mathcal{Y}$  is in  $\mathcal{B}_\varepsilon$ . For the inverse direction, consider any  $\nu \in \mathcal{B}_\varepsilon$  since we have assumed that  $\mathcal{B}_\varepsilon$  is non-empty. By the definition of  $\mathcal{B}_\varepsilon$ , one has  $\mathcal{W}_c(\hat{\mu}, \nu) \leq \varepsilon$ . The infimum in  $\mathcal{W}_c(\hat{\mu}, \nu)$  is attained by some  $\pi$ . One can check that the three conditions above hold for this transport plan  $\pi$ . Finally, note that when these three conditions hold, one has

$$\begin{aligned}\inf_{\substack{\lambda \geq 0, \gamma \in \Gamma, \\ \beta \in C_b(\Omega_{1:T})}} \mathcal{L}(\pi, \lambda, \gamma, \beta) &= \int_{\mathcal{X} \times \mathcal{Y}} f(y) \pi(dx, dy) + \lambda [\varepsilon - \int_{\mathcal{X} \times \mathcal{Y}} c(x, y) \pi(dx, dy)] \\ &= \int_{\mathcal{Y}} f(y) \nu(dy).\end{aligned}$$

It is immediate that

$$\sup_{\pi \in \mathcal{P}(\mathcal{X} \times \mathcal{Y})} \inf_{\substack{\lambda \geq 0, \gamma \in \Gamma, \\ \beta \in C_b(\Omega_{1:T})}} \mathcal{L}(\pi, \lambda, \gamma, \beta) = \sup_{\nu \in \mathcal{B}_\varepsilon} \int_{\mathcal{Y}} f(y) \nu(dy) = J(\varepsilon; \hat{\mu}).$$

Next, we consider the RHS. Rearranging the terms in  $\mathcal{L}$  gives

$$\mathcal{L}(\pi, \lambda, \gamma, \beta) = \lambda \varepsilon + \int_{\mathcal{X}} \beta(x) \hat{\mu}(dx) + \int_{\mathcal{X} \times \mathcal{Y}} (f(y) - \beta(x) - \lambda c(x, y) + \gamma(x, y)) \pi(dx, dy).$$

For the inner supremum of  $\mathcal{L}$  over  $\pi \in \mathcal{P}(\mathcal{X} \times \mathcal{Y})$  on the RHS, since  $\pi$  can choose arbitrary feasible marginal on the  $\mathcal{Y}$  side, it will take the supremum as

$$\begin{aligned}
& \sup_{\pi \in \mathcal{P}(\mathcal{X} \times \mathcal{Y})} \mathcal{L}(\pi, \lambda, \gamma, \beta) \\
&= \lambda \varepsilon + \int_{\mathcal{X}} \beta(x) \hat{\mu}(dx) + \sup_{x \in \mathcal{X}, y \in \mathcal{Y}} \{f(y) - \beta(x) - \lambda c(x, y) + \gamma(x, y)\} \\
&= \lambda \varepsilon + \int_{\mathcal{X}} \beta(x) \hat{\mu}(dx) + \sup_{x \in \mathcal{X}} \left\{ \sup_{y \in \mathcal{Y}} \{f(y) - \lambda c(x, y) + \gamma(x, y)\} - \beta(x) \right\} \\
&= \lambda \varepsilon + \int_{\mathcal{X}} \left[ \beta(x) + \sup_{x \in \mathcal{X}} \left\{ \sup_{y \in \mathcal{Y}} \{f(y) - \lambda c(x, y) + \gamma(x, y)\} - \beta(x) \right\} \right] \hat{\mu}(dx) \\
&\geq \lambda \varepsilon + \int_{\mathcal{X}} \sup_{y \in \mathcal{Y}} \{f(y) - \lambda c(x, y) + \gamma(x, y)\} \hat{\mu}(dx) \\
&= \lambda \varepsilon + \int_{\mathcal{X}} F(x; \lambda, \gamma) \hat{\mu}(dx).
\end{aligned}$$

The second equality uses the fact that we can take supremum over  $y$  first and then take supremum over  $x$ . The third equality holds since the last term is independent of  $x$  after taking supremum. The inequality is immediate when one notices that  $\sup(a - b) \geq a - b$ . Therefore, the RHS satisfies

$$\inf_{\substack{\lambda \geq 0, \gamma \in \Gamma, \\ \beta \in C_b(\Omega_{1:T})}} \sup_{\pi \in \mathcal{P}(\mathcal{X} \times \mathcal{Y})} \mathcal{L}(\pi, \lambda, \gamma, \beta) \geq \inf_{\lambda \geq 0, \gamma \in \Gamma} \lambda \varepsilon + \int_{\mathcal{X}} F(x; \lambda, \gamma) \hat{\mu}(dx) = D(\varepsilon; \hat{\mu}).$$

Together with results on the LHS, we obtain that  $J(\varepsilon; \hat{\mu}) \geq D(\varepsilon; \hat{\mu})$ . Observing that the weak duality  $J(\varepsilon; \hat{\mu}) \leq D(\varepsilon; \hat{\mu})$  holds by applying the definition of  $F$  directly, we have proved the strong duality that  $J(\varepsilon; \hat{\mu}) = D(\varepsilon; \hat{\mu})$ .

In general, when  $f$  is u.s.c. and  $c(x, y)$  is l.s.c., one can use the approximation arguments in Blanchet and Murthy (2019, Proposition 2), thanks to the compactness of  $\mathcal{X} \times \mathcal{Y}$ , a non-decreasing sequence of continuous functions approximating  $c(x, y)$  pointwisely, and a non-increasing sequence of continuous functions approximating  $f$  pointwisely.

The existence of a primal optimizer  $\nu^* \in \mathcal{B}_\varepsilon$  for  $J(\varepsilon; \hat{\mu})$  follows immediately from the fact that  $\mathcal{B}_\varepsilon$  is a compact subset of  $\mathcal{P}(\mathcal{X} \times \mathcal{Y})$  equipped with the weak topology.  $\square$

From the proof of Theorem 3.2, one can see that  $\pi$  will take the supremum over  $x$  and  $y$  pathwisely. It may lead to extreme cases with conservative worst-case scenarios that are unlikely to happen. We discuss more on this point later in Section 3.2.

As a side note, the minimization over  $g_{l,t}$  can be equivalently formulated as over martingales by Backhoff-Veraguas et al. (2017, Proposition 2.4). Let  $\mathcal{F}^{\mathcal{X}}$  be the filtration generated by the coordinate process on  $\mathcal{X}$ . The corresponding test function space is

$$\begin{aligned}
\Gamma' := \left\{ \gamma' : \mathcal{X} \times \mathcal{Y} \rightarrow \mathbb{R} \mid \gamma'(x, y) = \sum_{l=1}^L \sum_{t=1}^{T-1} h_{l,t}(y_{1:t}) \left[ M_{l,t+1}(x_{1:t+1}) - M_{l,t}(x_{1:t}) \right], \text{ with} \right. \\
\left. h_{l,t}, M_{l,t} \in C_b(\Omega_{1:t}), M_l \text{ an } \mathcal{F}^{\mathcal{X}}\text{-martingale, and some positive integer } L \in \mathbb{N} \right\}.
\end{aligned}$$

The proof of the following corollary is the same as Theorem 3.2, with  $\Gamma$  replaced by  $\Gamma'$ , and thus is omitted.

**Corollary 3.3.** *Under assumptions of Theorem 3.2,  $D(\varepsilon; \hat{\mu})$  has another representation as*

$$D(\varepsilon; \hat{\mu}) = \inf_{\lambda \geq 0, \gamma' \in \Gamma'} \lambda \varepsilon + \int_{\mathcal{X}} F(x; \lambda, \gamma') \hat{\mu}(dx) \tag{3.3}$$

with

$$F(x; \lambda, \gamma') = \sup_{y \in \mathcal{Y}} \{f(y) - \lambda c(x, y) + \gamma'(x, y)\}.$$

### 3.2 Motivating example

Is there any significant difference between COT and OT primal optimizers? When do they share a common primal optimizer? Before introducing numerical algorithms for general cases, we first consider a simple example with explicit solutions to understand the distinct features between COT and OT. Besides, we show that COT and OT can share a common optimizer when the cost and the objective are separable. More importantly and perhaps surprisingly, we highlight that the OT (and even COT) formulation may not find very different temporal structures than the reference measure. It motivates us to introduce a framework that can incorporate the structural information available.

Let the time step  $T = 2$  and the domain  $\mathcal{X} = \mathcal{Y} = [-1, 1]^2$ . Suppose the reference measure  $\hat{\mu} = 0.2\delta_{(0,1)} + 0.8\delta_{(0,-1)}$ . Equivalently,  $x_1 = 0$  with probability one.  $x_2 = 1$  with probability 0.2 and  $x_2 = -1$  with probability 0.8. Suppose the cost function  $c(x, y) = \mathbf{1}_{\{x_2 \neq y_1\}}$ , which is l.s.c.. Consider an objective  $f((x_1, x_2)) = x_1$  that only focuses on the first time point. Then the risk under the reference measure is

$$\int_{\mathcal{X}} f(x) \hat{\mu}(dx) = \int_{\mathcal{X}} x_1 \hat{\mu}(dx) = 0.$$

Let the radius  $\varepsilon = 0.2$ . By Theorem 3.2 with  $\gamma(x, y) \equiv 0$ , the dual problem of the OT formulation is

$$\begin{aligned} & \min_{\lambda \geq 0} \lambda \varepsilon + \int_{\mathcal{X}} \sup_{y_1 \in [-1, 1]} (y_1 - \lambda \mathbf{1}_{\{x_2 \neq y_1\}}) \hat{\mu}(dx_2) \\ &= \min_{\lambda \geq 0} \left\{ 0.2\lambda + 0.2 \sup_{y_1 \in [-1, 1]} (y_1 - \lambda \mathbf{1}_{\{y_1 \neq 1\}}) + 0.8 \sup_{y_1 \in [-1, 1]} (y_1 - \lambda \mathbf{1}_{\{y_1 \neq -1\}}) \right\} \\ &= \min_{\lambda \geq 0} \left\{ 0.2\lambda + 0.2 \times 1 + 0.8 \times (-1) \right\} = -0.6. \end{aligned}$$

Thus, the worst-case measure  $\nu^*$  will assign  $Y_1 = X_2$ , where we use capitalized letters to highlight random variables. It relies on the information from the future time, while OT does not punish this anticipative choice. Besides, note that the dual value  $-0.6$  is smaller than the reference case of 0, since  $c(x, x) \neq 0$ .

For the COT problem,  $\nu \in \mathcal{B}_\varepsilon$  if and only if there exists a causal transport plan  $\pi \in \Pi_c(\hat{\mu}, \nu)$  and  $\pi(Y_1 \neq X_2) \leq 0.2$ . The only information that  $Y_1$  can use to predict  $X_2$  is from  $X_1$ . However,  $X_1$  is not helpful in predicting  $X_2$  since  $\hat{\mu}$  is separable. Then for any causal transport plan  $\pi$ , we have

$$\begin{aligned} \pi(Y_1 \neq X_2) &= \pi(Y_1 \neq 1 | X_2 = 1) \hat{\mu}(X_2 = 1) + \pi(Y_1 \neq -1 | X_2 = -1) \hat{\mu}(X_2 = -1) \\ &= 0.2\nu(Y_1 \neq 1) + 0.8\nu(Y_1 \neq -1) = 1 - 0.2\nu(Y_1 = 1) - 0.8\nu(Y_1 = -1) \leq 0.2. \end{aligned}$$

On the other hand,  $\nu(Y_1 = 1) + \nu(Y_1 = -1) \leq 1$ . One must have  $\nu(Y_1 = -1) = 1$ . Then the worst-case value is  $-1$ , which is also smaller than the reference and the OT case. In general, the COT, OT and reference primal values can be arbitrarily distinct.

We can also obtain the same conclusion from the dual representation. For a function  $g_l \in C_b([-1, 1]^2)$ , denote the difference  $G_l(x_2; g) := g_l(x_1, x_2) - \int_{x_2} g_l(x_1, x_2) \hat{\mu}(dx_2 | x_1) = g_l(0, x_2) - 0.2g_l(0, 1) - 0.8g_l(0, -1)$ .

The dual problem of COT is

$$\begin{aligned}
& \min_{\lambda \geq 0, \gamma \in \Gamma} \lambda \varepsilon + \int_{\mathcal{X}} \sup_{y_1 \in [-1, 1]} (y_1 - \lambda \mathbf{1}_{\{x_2 \neq y_1\}} + \gamma(x, y)) \hat{\mu}(dx_2) \\
&= \min_{\substack{\lambda \geq 0, L \in \mathbb{N}, \\ h_l \in C_b([-1, 1]), \\ g_l \in C_b([-1, 1]^2)}} \left\{ 0.2\lambda + \int_{\mathcal{X}} \sup_{y_1 \in [-1, 1]} (y_1 - \lambda \mathbf{1}_{\{x_2 \neq y_1\}} + \sum_{l=1}^L h_l(y_1) G_l(x_2; g)) \hat{\mu}(dx_2) \right\} \\
&= \min_{\lambda \geq 0, L \in \mathbb{N}, h_l, g_l} \left\{ 0.2\lambda + 0.2 \sup_{y_1 \in [-1, 1]} (y_1 - \lambda \mathbf{1}_{\{y_1 \neq 1\}} + \sum_{l=1}^L h_l(y_1) G_l(1; g)) \right. \\
&\quad \left. + 0.8 \sup_{y_1 \in [-1, 1]} (y_1 - \lambda \mathbf{1}_{\{y_1 \neq -1\}} + \sum_{l=1}^L h_l(y_1) G_l(-1; g)) \right\}.
\end{aligned}$$

When  $X_2 = -1$ ,  $Y_1$  is forced to be  $-1$ . Otherwise, minimizing over  $\lambda$  will lead to  $-\infty$ . When  $X_2 = 1$ , if  $Y_1 \neq -1$ , then minimizing over  $h_l$  and  $g_l$  will also lead to  $-\infty$ . In summary,  $Y_1 \equiv -1$  is the only choice to prevent it from being  $-\infty$ .

Besides, note that if we set  $\varepsilon < 0.2$ , the causal Wasserstein ball  $\mathcal{B}_\varepsilon$  will be empty. The assumption that  $\mathcal{B}_\varepsilon$  is non-empty in Theorem 3.2 is then necessary.

The previous example shows COT and OT have different optimizers in general. The following corollary investigates another side. When the objective and the cost are separable, COT and OT share a common optimizer.

**Corollary 3.4.** *Suppose  $f(y) = \sum_{t=1}^T f_t(y_t)$  and  $c(x, y) = \sum_{t=1}^T c_t(x_t, y_t)$  satisfying  $c_t \geq 0$  and  $c_t(x_t, x_t) = 0$ . Assumptions in Theorem 3.2 hold. Then COT and OT share a common optimizer for  $J(\varepsilon; \hat{\mu})$ . More precisely, there is a measurable map  $L_t : \Omega_t \rightarrow \Omega_t$  for each  $t \in [T]$ . A worst-case measure  $\nu^*$  is induced by  $Y_t = L_t(X_t)$ .*

*Proof.* With  $c_t(x_t, x_t) = 0$ ,  $\mathcal{B}_\varepsilon$  is non-empty since at least the reference measure  $\hat{\mu}$  is in it. We can apply Theorem 3.2 to the OT formulation and obtain

$$\begin{aligned}
J(\varepsilon; \hat{\mu}) = D(\varepsilon; \hat{\mu}) &= \inf_{\lambda \geq 0} \lambda \varepsilon + \int_{\mathcal{X}} \sup_{y \in \mathcal{Y}} \{f(y) - \lambda c(x, y)\} \hat{\mu}(dx) \\
&= \inf_{\lambda \geq 0} \lambda \varepsilon + \int_{\mathcal{X}} \sum_{t=1}^T \sup_{y_t \in \Omega_t} \{f_t(y_t) - \lambda c_t(x_t, y_t)\} \hat{\mu}(dx).
\end{aligned}$$

There exists a maximizer  $y = L(x)$ . Note that  $L$  may not be unique. But it can be chosen measurable, see Bertsekas and Shreve (1996, Proposition 7.50(b)). In view of the separable structure of  $f(y)$  and  $c(x, y)$ , we further know that  $L$  is separable with  $y_t = L_t(x_t)$ .

First, the OT primal value is not less than the COT one. For the inverse direction, observe that  $L_t$  does not violate the non-anticipativeness. Therefore, the COT primal value is not less than the OT one. We prove the result as desired.  $\square$

Corollary 3.4 implies that with the separable cost and objective, the worst-case scenario can be deduced separately and does not rely on the future values. It exhausts the current state  $x_t$  to find the worst-case  $y_t$ . For example, if we consider  $f(y)$  as the sum of  $y$  and  $c(x, y)$  as the  $l_1$  norm, then the worst-case scenario is simply the reference measure shifted by a constant depending on the radius  $\varepsilon$ . Thus, the temporal structure of  $x$  and  $y$  is the same. In this sense, we claim that COT and OT rely on the reference measure *pointwisely and pathwisely*, instead of jointly on samples. This feature is conservative and somehow undesired when some data points have abnormal spikes or observation errors. Motivated by this fact, we further embed some structural information into alternative measures and refer to the framework as the structural COT or SCOT for short.

### 3.3 Incorporating structural information

Suppose structural information is available and can be modeled with a non-empty subset  $\mathcal{V} \subset \mathcal{P}(\mathcal{Y})$ . Denote the primal problem with structural information as

$$J(\varepsilon; \hat{\mu}, \mathcal{V}) := \sup_{\nu \in \mathcal{B}_\varepsilon \cap \mathcal{V}} \int_{\mathcal{Y}} f(y) \nu(dy). \quad (3.4)$$

Commonly, one can restrict  $\mathcal{V}$  to be a parametric space, encoded with structural information that the DM knows a priori. Then we can regard the SCOT framework as robust estimation of parametric models. If we choose  $\mathcal{V}$  as the set of all Borel probability measures on  $\mathcal{Y}$ , it reduces to the COT framework (2.6). Similarly, we have the following dual representation for (3.4). Note that the domains  $\mathcal{X}$  and  $\mathcal{Y}$  need not be bounded.

**Theorem 3.5.** *Suppose Assumption 3.1 holds,  $\mathcal{X}$  and  $\mathcal{Y}$  are closed,  $f$  is bounded from above, and  $\mathcal{B}_\varepsilon$  is non-empty for certain  $\varepsilon > 0$ . Then  $J(\varepsilon; \hat{\mu}, \mathcal{V}) = D(\varepsilon; \hat{\mu}, \mathcal{V})$ , where*

$$D(\varepsilon; \hat{\mu}, \mathcal{V}) = \sup_{\nu \in \mathcal{V}} \inf_{\substack{\lambda \geq 0, \\ \gamma \in \Gamma}} \left\{ \lambda \varepsilon + \sup_{\pi \in \Pi(\hat{\mu}, \nu)} \int_{\mathcal{X} \times \mathcal{Y}} [f(y) - \lambda c(x, y) + \gamma(x, y)] \pi(dx, dy) \right\}. \quad (3.5)$$

*Proof.* We deal with the general  $f(y)$  and  $c(x, y)$  satisfying Assumption 3.1 directly. Fix  $\nu \in \mathcal{V}$ , introduce the Lagrangian

$$\mathcal{L}(\pi, \lambda, \gamma; \nu) := \int_{\mathcal{X} \times \mathcal{Y}} (f(y) + \gamma(x, y)) \pi(dx, dy) + \lambda \left[ \varepsilon - \int_{\mathcal{X} \times \mathcal{Y}} c(x, y) \pi(dx, dy) \right].$$

By Santambrogio (2015, Theorem 1.7),  $\Pi(\hat{\mu}, \nu)$ , the set of transport plans between  $\hat{\mu}$  and  $\nu$ , is compact under the weak topology. Since  $f$  is u.s.c. and bounded from above,  $\gamma(x, y)$  is continuous and bounded,  $c(x, y)$  is l.s.c. and non-negative, we obtain that  $\mathcal{L}$  is u.s.c. in  $\pi$  by Santambrogio (2015, Lemma 1.6). Consider the space  $C_b(\mathcal{X} \times \mathcal{Y})$  endowed with uniform topology and  $\lambda \geq 0$  with the Euclidean topology, one has that  $\mathcal{L}$  is continuous in  $\lambda$  and  $\gamma$ . Similarly,  $\mathcal{L}$  is linear in  $\pi$  for given  $(\lambda, \gamma)$  and linear in  $(\lambda, \gamma)$  for given  $\pi$ . Sion's minimax theorem shows that

$$\sup_{\pi \in \Pi(\hat{\mu}, \nu)} \inf_{\substack{\lambda \geq 0, \\ \gamma \in \Gamma}} \mathcal{L}(\pi, \lambda, \gamma; \nu) = \inf_{\substack{\lambda \geq 0, \\ \gamma \in \Gamma}} \sup_{\pi \in \Pi(\hat{\mu}, \nu)} \mathcal{L}(\pi, \lambda, \gamma; \nu). \quad (3.6)$$

As in Theorem 3.2, one can verify that

$$J(\varepsilon; \mathcal{V}) = \sup_{\nu \in \mathcal{V}} \sup_{\pi \in \Pi(\hat{\mu}, \nu)} \inf_{\substack{\lambda \geq 0, \\ \gamma \in \Gamma}} \mathcal{L}(\pi, \lambda, \gamma; \nu)$$

Simplifying the RHS of (3.6), we obtain  $D(\varepsilon; \hat{\mu}, \mathcal{V})$  in (3.5) after taking supremum over  $\nu \in \mathcal{V}$ .  $\square$

Similarly, the infimum over  $\gamma \in \Gamma$  can be replaced by  $\gamma' \in \Gamma'$ .

One advantage of the dual representation (3.5) is the inner supremum over  $\pi \in \Pi(\hat{\mu}, \nu)$  is closely connected with the classic Wasserstein distance. Indeed, after moving the negative sign out, we have

$$\begin{aligned} & \sup_{\pi \in \Pi(\hat{\mu}, \nu)} \int_{\mathcal{X} \times \mathcal{Y}} [f(y) - \lambda c(x, y) + \gamma(x, y)] \pi(dx, dy) \\ &= - \inf_{\pi \in \Pi(\hat{\mu}, \nu)} \int_{\mathcal{X} \times \mathcal{Y}} [-f(y) + \lambda c(x, y) - \gamma(x, y)] \pi(dx, dy) \\ &=: -\mathcal{W}(\hat{\mu}, \nu; \lambda, \gamma). \end{aligned} \quad (3.7)$$

Section 4.4 will present several algorithms to approximate Wasserstein distance and thus the inner supremum over  $\pi$ .

## 4 Sample complexity and optimization

The dual representation of COT (3.1) and SCOT (3.5) poses several essential difficulties to optimization. In COT, the inner maximization over  $y$  is non-concave in general, which is NP-hard already. The outer minimization is over  $\lambda$  and an infinite-dimensional test function space, which also appears in SCOT. To reduce the minimization over test functions to a finite-dimensional problem, we adopt neural networks to model elements from the test function space. The motivations are twofold. First, compared with the discrete scheme in Acciaio et al. (2021); Zhou et al. (2021) which often suffers from the curse of dimensionality, the parametric formulation scales well when the sample size increases. The test functions learned may also demonstrate some meaningful patterns. Another motivation is the approximation capability of neural networks and the modern computational tools available. In Section 4.2, we first prove the sample complexity of COT with tools from Rademacher complexity. In Section 4.3, we provide finite sample guarantee for SCOT. Optimization algorithms are discussed later in Section 4.4. As preparation, we first introduce the adapted empirical measure in Backhoff-Veraguas et al. (2020) that resolves a flaw of classic empirical measure.

In this section, we further assume

**Assumption 4.1.**  $\Omega_t$  is a bounded sub-interval as  $\Omega_t = [a, b]$  for all  $t \in [T]$ .  $f$  and  $c(x, y)$  are continuous and satisfy Assumption 3.1.

The sample complexity analysis relies on the consistency results from Backhoff-Veraguas et al. (2020), which holds for closed interval domains. Moreover, the convergence analysis of Rademacher complexity also needs a compact domain.

### 4.1 Adapted empirical measures

The reference measure  $\hat{\mu}$  is usually chosen as the empirical measure  $\hat{\mu}_N$  with  $N$  observed paths  $x_{1:T}^n$ , i.i.d. from an underlying measure  $\mu$ . As noted in Pflug and Pichler (2016); Backhoff-Veraguas et al. (2020),  $\mathcal{W}_c(\hat{\mu}_N, \mu) \rightarrow 0$  may not hold when same size  $N \rightarrow \infty$ . To understand this undesired property, consider the measure  $\mu$  that has a density function with respect to the Lebesgue measure. The probability that two observed samples coincide at some time point is zero. Then the empirical measure is Dirac measure almost surely. Once we know the starting point, the whole path is known. There will be no penalty from  $h_{l,t}$  and  $g_{l,t}$ . Thus, convergence in  $\mathcal{W}_c$  fails.

To resolve this issue, Backhoff-Veraguas et al. (2020) proposes a quantization method. Divide  $\Omega_t = [a, b]$  into disjoint unions of  $N^{1/(T+1)}$  sub-intervals with a length of  $(b - a)/N^{1/(T+1)}$ . Let  $\varphi_N : [a, b] \rightarrow [a, b]$  map each sub-interval to its center. Define the **adapted** empirical measure as

$$\hat{\mu}(dx_{1:T}|N, \varphi_N) := \frac{1}{N} \sum_{n=1}^N \delta_{\varphi_N(x_{1:T}^n)}.$$

In this notation, the first  $N$  means  $N$  samples are used.  $\varphi_N$  highlight the role of the partition map. Denote the partition formulated by  $\varphi_N$  on  $[a, b]$  as

$$\Phi_N := \{\varphi_N^{-1}(x) : x \in \varphi_N([a, b])\}.$$

For every  $1 \leq t \leq T - 1$ , the product of sub-intervals formulates

$$\Phi_{N,t} := \left\{ \prod_{1 \leq s \leq t} B_s : B_s \in \Phi_N \right\}.$$

With a slight abuse of notation, we interpret  $\varphi_N^{-1}(x_{1:t})$  as the product of sub-intervals when  $\varphi_N^{-1}$  is applied element-wisely.

Recall that  $\mu(dx_{t+1:T}|x_{1:t})$  is the true conditional measure. With a set  $A_t \in \Phi_{N,t}$ , we can define the **adapted** empirical conditional measure as

$$\hat{\mu}(dx_{t+1:T}|A_t, N, \varphi_N) := \frac{1}{|\{x_{1:t}^n \in A_t, n \in [N]\}|} \sum_{x_{1:t}^n \in A_t, n \in [N]} \delta_{\varphi_N(x_{t+1:T}^n)}.$$

Besides, we also need the following notation for later use:

$$\hat{\mu}(dx_{t+1:T}|A_t, N, \text{id}) := \frac{1}{|\{x_{1:t}^n \in A_t, n \in [N]\}|} \sum_{x_{1:t}^n \in A_t, n \in [N]} \delta_{x_{t+1:T}^n}.$$

Intuitively speaking, with quantization, the sample paths are not fully known after the first time point.

## 4.2 Rademacher complexity

In this subsection, we consider the dual problem of COT with the test function space in Theorem 3.2. To make notations compact, denote  $\theta$  as  $\{h_{l,t}, g_{l,t}, l \in [L]\}$  and  $\lambda \geq 0$ . In the language of machine learning theory, a family of  $\theta$ , denoted as  $\Theta_k$ , is known as a hypothesis set. Recall the dual problem of COT in (3.1). When we set  $\hat{\mu}$  as the adapted empirical measure  $\hat{\mu}(dx_{1:T}|N, \varphi_N)$ , the dual problem (3.1) minimizes

$$\begin{aligned} & D(\theta, \varepsilon; \hat{\mu} \circ \varphi_N^{-1}) \\ &:= \int \sup_{y \in \mathcal{Y}} \left\{ f(y) - \lambda c(x, y) + \sum_{l=1}^L \sum_{t=1}^{T-1} h_{l,t}(y_{1:t}) [g_{l,t}(x_{1:T}) \right. \\ &\quad \left. - \int g_{l,t}(x_{1:T}) \hat{\mu}(dx_{t+1:T}|\varphi_N^{-1}(x_{1:t}), N, \varphi_N)] \right\} \hat{\mu}(dx_{1:T}|N, \varphi_N) + \lambda \varepsilon \\ &= \int \sup_{y \in \mathcal{Y}} \left\{ f(y) - \lambda c(\varphi_N(x), y) + \sum_{l=1}^L \sum_{t=1}^{T-1} h_{l,t}(y_{1:t}) [g_{l,t}(\varphi_N(x_{1:T})) \right. \\ &\quad \left. - \int g_{l,t}(\varphi_N(x_{1:T})) \hat{\mu}(dx_{t+1:T}|\varphi_N^{-1}(x_{1:t}), N, \text{id})] \right\} \hat{\mu}(dx_{1:T}|N, \text{id}) + \lambda \varepsilon. \end{aligned}$$

The second inequality follows from the push-forward property. We use  $\hat{\mu} \circ \varphi_N^{-1}$  to highlight the adapted empirical measure for abbreviation. Let  $\Theta$  be the hypothesis set with  $\Gamma$  and  $\lambda \geq 0$ . Note that

$$\inf_{\theta \in \Theta} D(\theta, \varepsilon; \hat{\mu} \circ \varphi_N^{-1}) = D(\varepsilon; \hat{\mu} \circ \varphi_N^{-1}),$$

with RHS defined in Theorem 3.2.

A function used in the middle of proofs is

$$\begin{aligned} D(\theta, \varepsilon; \mu \circ \varphi_N^{-1}) &:= \int \sup_{y \in \mathcal{Y}} \left\{ f(y) - \lambda c(\varphi_N(x), y) + \sum_{l=1}^L \sum_{t=1}^{T-1} h_{l,t}(y_{1:t}) [g_{l,t}(\varphi_N(x_{1:T})) \right. \\ &\quad \left. - \int g_{l,t}(\varphi_N(x_{1:T})) \mu(dx_{t+1:T}|\varphi_N^{-1}(x_{1:t}))] \right\} \mu(dx_{1:T}) + \lambda \varepsilon. \end{aligned}$$

The probability measure is the true  $\mu$  while the partition map remains in the integral. Besides, let  $D(\theta, \varepsilon; \mu)$  be the function minimized under the true measure  $\mu$  and without the partition map.

We recall the definition of (empirical) Rademacher complexity from Mohri et al. (2018, Definition 3.2, Chapter 3):

**Definition 4.2.** The empirical Rademacher complexity of a hypothesis set  $\mathcal{G}$  with respect to a fixed sample  $S = (x_{1:T}^1, \dots, x_{1:T}^N)$  of size  $N$  is defined as

$$\mathcal{R}_S(\mathcal{G}; N) = \mathbb{E}_\sigma \left[ \sup_{g \in \mathcal{G}} \frac{1}{N} \sum_{i=1}^N \sigma_i g(x^i) \right], \quad (4.1)$$

where  $\sigma = (\sigma_1, \dots, \sigma_N)$  with  $\sigma_i$ s independent uniform random variables taking values in  $\{-1, +1\}$ .

For any positive integer  $N$ , the Rademacher complexity of  $\mathcal{G}$  is the expectation of the empirical Rademacher complexity over all samples of size  $N$  drawn according to  $\mu$ :

$$\mathcal{R}(\mathcal{G}; N) = \mathbb{E}_S[\mathcal{R}_S(\mathcal{G}; N)]. \quad (4.2)$$

Let  $\Theta_k \subset \Theta$  be a given hypothesis set. Denote  $\mathcal{R}(\mathcal{G}_k \circ \varphi_N; N^{1/T})$  as the Rademacher complexity of the family of functions  $g_{l,t}(\varphi_N(\cdot))$ , with  $g_{l,t}$  from  $\Theta_k$  and the sample size as  $N^{1/T}$ .  $D(\theta, \varepsilon; \hat{\mu} \circ \varphi_N^{-1})$  depends on the hypothesis set  $\Theta_k$  via  $F$  in (3.1). We need to consider  $\mathcal{R}(F(\Theta_k \circ \varphi_N); N)$  as the Rademacher complexity of the family of the function  $F$  composited with  $g_{l,t}(\varphi_N(\cdot))$  and  $h_{l,t}(\varphi_N(\cdot))$  from  $\Theta_k$ .

Our first technical result is to derive general learning guarantees for  $\Theta_k$ . Define a function

$$r(x) := 2\mathcal{R}(\mathcal{G}_k \circ \varphi_N; x) + 2C_g \sqrt{\frac{\ln(2/\delta)}{2x}}, \quad x \in [0, \infty), \quad (4.3)$$

for later use in the proof.  $C_g$  is a constant to uniformly bound all  $g_{l,t}$  in  $\Theta_k$  and independent of  $x$ . The main difficulty is that the adapted empirical measures appear in the integral with functions  $g_{l,t}$ .

**Lemma 4.3.** Suppose

1. Assumption 4.1 holds;
2. All functions  $h_{l,t}$  and  $g_{l,t}$  in the hypothesis set  $\Theta_k$  are uniformly bounded by a large enough constant  $C_{h,g}$ , independent of sample size  $N$ ;
3.  $xr(x)$  is concave on  $[0, \infty)$  and  $r(x)$  is decreasing on  $[0, \infty)$ .

Then with probability at least  $1 - \delta$  over the draw of i.i.d. sample of  $\mu$ , the generalization error is bounded by

$$\begin{aligned} \sup_{\theta \in \Theta_k} |D(\theta, \varepsilon; \mu \circ \varphi_N^{-1}) - D(\theta, \varepsilon; \hat{\mu} \circ \varphi_N^{-1})| &\leq 2\mathcal{R}(F(\Theta_k \circ \varphi_N); N) + 2C_{h,g} \sqrt{\frac{\ln(2/\delta)}{2N}} \\ &\quad + C_{h,g} r(N^{1/T}). \end{aligned}$$

*Proof.* To ease the notation, let  $f^c(x, y, \lambda) := f(y) - \lambda c(x, y)$ . With the definition of  $D(\theta, \varepsilon; \mu \circ \varphi_N^{-1})$  and  $D(\theta, \varepsilon; \hat{\mu} \circ \varphi_N^{-1})$ , by adding and deducting a common term, an application of the

triangle inequality gives

$$\begin{aligned}
& |D(\theta, \varepsilon; \mu \circ \varphi_N^{-1}) - D(\theta, \varepsilon; \hat{\mu} \circ \varphi_N^{-1})| \\
& \leq \left| \int \sup_{y \in \mathcal{Y}} \left\{ \sum_{l=1}^L \sum_{t=1}^{T-1} h_{l,t}(y_{1:t}) \left[ g_{l,t}(\varphi_N(x_{1:T})) - \int g_{l,t}(\varphi_N(x_{1:T})) \mu(dx_{t+1:T} | \varphi_N^{-1}(x_{1:t})) \right] \right. \right. \\
& \quad \left. \left. + f^c(\varphi_N(x), y, \lambda) \right\} \mu(dx_{1:T}) \right. \\
& \quad \left. - \int \sup_{y \in \mathcal{Y}} \left\{ \sum_{l=1}^L \sum_{t=1}^{T-1} h_{l,t}(y_{1:t}) \left[ g_{l,t}(\varphi_N(x_{1:T})) - \int g_{l,t}(\varphi_N(x_{1:T})) \mu(dx_{t+1:T} | \varphi_N^{-1}(x_{1:t})) \right] \right. \right. \\
& \quad \left. \left. + f^c(\varphi_N(x), y, \lambda) \right\} \hat{\mu}(dx_{1:T} | N, \text{id}) \right| \\
& \quad + \left| \int \sup_{y \in \mathcal{Y}} \left\{ \sum_{l=1}^L \sum_{t=1}^{T-1} h_{l,t}(y_{1:t}) \left[ g_{l,t}(\varphi_N(x_{1:T})) - \int g_{l,t}(\varphi_N(x_{1:T})) \hat{\mu}(dx_{t+1:T} | \varphi_N^{-1}(x_{1:t}), N, \text{id}) \right] \right. \right. \\
& \quad \left. \left. + f^c(\varphi_N(x), y, \lambda) \right\} \hat{\mu}(dx_{1:T} | N, \text{id}) \right. \\
& \quad \left. - \int \sup_{y \in \mathcal{Y}} \left\{ \sum_{l=1}^L \sum_{t=1}^{T-1} h_{l,t}(y_{1:t}) \left[ g_{l,t}(\varphi_N(x_{1:T})) - \int g_{l,t}(\varphi_N(x_{1:T})) \mu(dx_{t+1:T} | \varphi_N^{-1}(x_{1:t})) \right] \right. \right. \\
& \quad \left. \left. + f^c(\varphi_N(x), y, \lambda) \right\} \hat{\mu}(dx_{1:T} | N, \text{id}) \right| \\
& =: \text{I} + \text{II}.
\end{aligned}$$

Recall the definition of  $F$ , part I is the difference between empirical averages and the expected value of  $F$ . Since the sample is i.i.d. drawn from  $\mu$  and continuous functions on compact subsets are bounded, then Mohri et al. (2018, Theorem 3.3) and Reppen and Soner (2020, Section 7.1) imply

$$\text{I} \leq 2\mathcal{R}(F(\Theta_k \circ \varphi_N); N) + 2C_{h,g} \sqrt{\frac{\ln(2/\delta)}{2N}}$$

holds with probability at least  $1 - \delta$ .

For part II, we claim that

$$\begin{aligned}
\text{II} & \leq C_h \int \sum_{l=1}^L \sum_{t=1}^{T-1} \left| \int g_{l,t}(\varphi_N(x_{1:T})) \hat{\mu}(dx_{t+1:T} | \varphi_N^{-1}(x_{1:t}), N, \text{id}) \right. \\
& \quad \left. - \int g_{l,t}(\varphi_N(x_{1:T})) \mu(dx_{t+1:T} | \varphi_N^{-1}(x_{1:t})) \right| \hat{\mu}(dx_{1:T} | N, \text{id}) \quad (4.4)
\end{aligned}$$

$$\leq C_h \sum_{t=1}^{T-1} \sum_{A_t \in \Phi_{N,t}} \hat{\mu}(A_t | N) \left\{ 2\mathcal{R}(\mathcal{G}_k \circ \varphi_N; n(A_t)) + 2C_g \sqrt{\frac{\ln(2/\delta)}{2n(A_t)}} \right\} \quad (4.5)$$

$$= C_h \sum_{t=1}^{T-1} \sum_{A_t \in \Phi_{N,t}} \hat{\mu}(A_t | N) r(n(A_t)). \quad (4.6)$$

$C_h$  is a large constant to bound all  $h_{l,t}$  in  $\Theta_k$ .  $\hat{\mu}(A_t | N)$  is the empirical probability on the set  $A_t$  when there are  $N$  sample paths.  $n(A_t)$  denotes the number of sample paths that fall into the set  $A_t$ . Thus, we have  $n(A_t) = N\hat{\mu}(A_t | N)$  and  $\sum_{A_t \in \Phi_{N,t}} n(A_t) = N$ .

Inequality (4.4) uses the property that  $F$  is Lipschitz in the integral of  $g_{l,t}$  with Lipschitz coefficient  $C_h$ . For inequality (4.5), first note that it is the same to use  $\hat{\mu}(dx_{t+1:T} | \varphi_N^{-1}(x_{1:t}), N, \varphi_N)$  in the place of  $\hat{\mu}(dx_{t+1:T} | \varphi_N^{-1}(x_{1:t}), N, \text{id})$  in (4.4). By Backhoff-Veraguas et al. (2020, Lemma 3.3), the law of  $\hat{\mu}(dx_{t+1:T} | \varphi_N^{-1}(x_{1:t}), N, \varphi_N)$  is the same as that of the empirical measure of

$\mu(dx_{t+1:T}|\varphi_N^{-1}(x_{1:t}))$  with sample size  $N\hat{\mu}(\varphi_N^{-1}(x_{1:t})|N)$ . Applying Mohri et al. (2018, Theorem 3.3) and Reppen and Soner (2020, Section 7.1) again, we obtain inequality (4.5) with sample size  $n(A_t)$  for each  $A_t$ .

With the definition of  $r(\cdot)$  in (4.3), note that  $xr(x)$  is concave on  $[0, \infty)$  and  $r(x)$  is decreasing on  $[0, \infty)$  under assumptions. Then

$$\begin{aligned} \sum_{A_t \in \Phi_{N,t}} \hat{\mu}(A_t|N) r(n(A_t)) &= \frac{|\Phi_{N,t}|}{N} \sum_{A_t \in \Phi_{N,t}} \frac{N\hat{\mu}(A_t|N)}{|\Phi_{N,t}|} r(N\hat{\mu}(A_t|N)) \\ &\leq \frac{|\Phi_{N,t}|}{N} \left( \sum_{A_t \in \Phi_{N,t}} \frac{N\hat{\mu}(A_t|N)}{|\Phi_{N,t}|} \right) r\left( \sum_{A_t \in \Phi_{N,t}} \frac{N\hat{\mu}(A_t|N)}{|\Phi_{N,t}|} \right) = r\left( \frac{N}{|\Phi_{N,t}|} \right) \leq r\left( \frac{N}{N^{(T-1)/T}} \right) \\ &= r(N^{1/T}). \end{aligned}$$

Summing up the results for I and II, we obtain the claim as desired.  $\square$

Under certain conditions on neural network parameters, the Rademacher complexity of many neural network architectures converges to zero when the sample size goes to infinity. For example, Golowich et al. (2018, Theorem 1) proved that the Rademacher complexity of fully-connected neural networks is of order  $O(1/\sqrt{N})$  with high probability. Wei and Ma (2019, Theorem G.1) proved relevant results for recurrent neural networks (RNNs) with the same order of  $O(1/\sqrt{N})$ . These results also validate Condition 3 in Lemma 4.3.

In the following lemma, we fix the hypothesis set  $\Theta_k$  and let the sample size goes to infinity. Then we can obtain the infimum of the dual problem over the hypothesis set  $\Theta_k$  and under the true measure  $\mu$ .

**Lemma 4.4.** *Given  $\Theta_k$ , suppose the Rademacher complexity in Lemma 4.3 converges to zero when sample size  $N \rightarrow \infty$  and Assumptions in Lemma 4.3 hold, then*

$$\lim_{N \rightarrow \infty} \inf_{\theta \in \Theta_k} D(\theta, \varepsilon; \hat{\mu} \circ \varphi_N^{-1}) = \inf_{\theta \in \Theta_k} D(\theta, \varepsilon; \mu),$$

with probability one.

*Proof.* Define

$$\theta_{k,N}^* \in \arg \min_{\theta \in \Theta_k} D(\theta, \varepsilon; \hat{\mu} \circ \varphi_N^{-1}), \quad \theta_k^* \in \arg \min_{\theta \in \Theta_k} D(\theta, \varepsilon; \mu)$$

be any minimizer. Since  $\sup_{u \in [a,b]} |u - \varphi_N(u)| \leq c/N^{1/(T+1)}$  for some constant  $c$ , for a given  $\eta > 0$ , there exists  $N_\eta$  such that when  $N \geq N_\eta$ ,

$$|D(\theta_k^*, \varepsilon; \mu \circ \varphi_N^{-1}) - D(\theta_k^*, \varepsilon; \mu)| \leq \eta/2, \quad (4.7)$$

$$|D(\theta_{k,N}^*, \varepsilon; \hat{\mu} \circ \varphi_N^{-1}) - D(\theta_{k,N}^*, \varepsilon; \mu)| \leq \eta/2. \quad (4.8)$$

The definition of  $\theta_{k,N}^*$  implies

$$D(\theta_{k,N}^*, \varepsilon; \hat{\mu} \circ \varphi_N^{-1}) \leq D(\theta_k^*, \varepsilon; \hat{\mu} \circ \varphi_N^{-1}). \quad (4.9)$$

Furthermore, for a given  $\delta > 0$ , Lemma 4.3 proves that

$$\begin{aligned} D(\theta_k^*, \varepsilon; \hat{\mu} \circ \varphi_N^{-1}) &\leq D(\theta_k^*, \varepsilon; \mu \circ \varphi_N^{-1}) + 2\mathcal{R}(F(\Theta_k \circ \varphi_N); N) + 2C_{h,g} \sqrt{\frac{\ln(2/\delta)}{2N}} + C_{h,g} r(N^{1/T}) \\ &\leq D(\theta_k^*, \varepsilon; \mu \circ \varphi_N^{-1}) + 2\mathcal{R}(F(\Theta_k \circ \varphi_N); N) + 2\mathcal{R}(\mathcal{G} \circ \varphi_N; N^{1/T}) + C \sqrt{\frac{\ln(2/\delta)}{N^{1/T}}} \\ &=: D(\theta_k^*, \varepsilon; \mu \circ \varphi_N^{-1}) + \mathcal{R}_N + C \sqrt{\frac{\ln(2/\delta)}{N^{1/T}}} \end{aligned} \quad (4.10)$$

holds with probability at least  $1 - \delta$ . Constant  $C$  is independent of sample size  $N$ . Combining (4.9), (4.10), and (4.8), one has

$$D(\theta_{k,N}^*, \varepsilon; \hat{\mu} \circ \varphi_N^{-1}) \leq D(\theta_k^*, \varepsilon; \mu) + \mathcal{R}_N + C \sqrt{\frac{\ln(2/\delta)}{N^{1/T}}} + \eta/2 \quad (4.11)$$

with probability at least  $1 - \delta$ .

In a similar manner, by invoking the definition of  $\theta_k^*$ , (4.8), and Lemma 4.3, we get

$$\begin{aligned} D(\theta_k^*, \varepsilon; \mu) &\leq D(\theta_{k,N}^*, \varepsilon; \mu) \leq D(\theta_{k,N}^*, \varepsilon; \mu \circ \varphi_N^{-1}) + \eta/2 \\ &\leq D(\theta_{k,N}^*, \varepsilon; \hat{\mu} \circ \varphi_N^{-1}) + \mathcal{R}_N + C \sqrt{\frac{\ln(2/\delta)}{N^{1/T}}} + \eta/2 \end{aligned} \quad (4.12)$$

with probability at least  $1 - \delta$ .

In view of (4.11) and (4.12), with probability at least  $1 - \delta$ , we have

$$|D(\theta_{k,N}^*, \varepsilon; \hat{\mu} \circ \varphi_N^{-1}) - D(\theta_k^*, \varepsilon; \mu)| \leq \mathcal{R}_N + C \sqrt{\frac{\ln(2/\delta)}{N^{1/T}}} + \eta/2. \quad (4.13)$$

For sufficiently large sample size  $N$ , we then pick  $\delta = \delta_N > 0$  such that

$$C \sqrt{\frac{\ln(2/\delta_N)}{N^{1/T}}} = \eta/2 \text{ or equivalently } \delta_N = 2 \exp \left[ - \frac{\eta^2 N^{1/T}}{4C^2} \right]. \quad (4.14)$$

Since  $\sum_N \delta_N < \infty$ , the Borel-Cantelli lemma implies that

$$\limsup_{N \rightarrow \infty} |D(\theta_{k,N}^*, \varepsilon; \hat{\mu} \circ \varphi_N^{-1}) - D(\theta_k^*, \varepsilon; \mu)| \leq \lim_{N \rightarrow \infty} \mathcal{R}_N + \eta/2 + \eta/2 = \eta,$$

with probability one. Since  $\eta$  is arbitrary, we prove the claim as desired.  $\square$

Finally, let the hypothesis set be large enough to approximate  $\Theta$ . Then we obtain the dual value with the true measure  $\mu$  and  $D(\varepsilon; \mu) = J(\varepsilon; \mu)$  by Theorem 3.2. Note that since  $\mu$  may not be in the causal Wasserstein ball without the assumption  $c(x, x) = 0, x \in \mathcal{X}$ , then  $J(\varepsilon; \mu) < \int_{\mathcal{X}} f(x) \mu(dx)$  can happen.

**Lemma 4.5.** *With the true measure  $\mu$ , suppose Assumptions in Lemma 4.4 hold. If a sequence of hypothesis sets  $\Theta_k$  can pointwisely approximate any bounded continuous functions when  $k \rightarrow \infty$ , then*

$$\lim_{k \rightarrow \infty} \inf_{\theta \in \Theta_k} D(\theta, \varepsilon; \mu) = \inf_{\theta \in \Theta} D(\theta, \varepsilon; \mu) = D(\varepsilon; \mu) = J(\varepsilon; \mu).$$

*Proof.* For any  $\varepsilon > 0$ , we can find  $\theta_\eta$  such that  $D(\theta_\eta, \varepsilon; \mu) \leq \inf_{\theta \in \Theta} D(\theta, \varepsilon; \mu) + \eta$ . By assumption, there exists a sequence of  $\theta_k \in \Theta_k$  approximating  $\theta_\eta$  pointwisely. Observing that  $F(x; \lambda, h, g)$  is continuous in  $x$  since it is the supremum of a continuous function (noting that  $h_{l,t}, g_{l,t}, f, c(x, y)$  are continuous) on a compact domain  $\mathcal{X} \times \mathcal{Y}$ . The dominated convergence theorem shows that

$$\lim_{k \rightarrow \infty} D(\theta_k, \varepsilon; \mu) = D(\theta_\eta, \varepsilon; \mu).$$

Then

$$\limsup_{k \rightarrow \infty} \inf_{\theta \in \Theta_k} D(\theta, \varepsilon; \mu) \leq \lim_{k \rightarrow \infty} D(\theta_k, \varepsilon; \mu) = D(\theta_\eta, \varepsilon; \mu) \leq \inf_{\theta \in \Theta} D(\theta, \varepsilon; \mu) + \eta. \quad (4.15)$$

The opposite direction  $\inf_{\theta \in \Theta} D(\theta, \varepsilon; \mu) \leq \inf_{\theta \in \Theta_k} D(\theta, \varepsilon; \mu)$  always holds. Since  $\eta$  is arbitrary in (4.15), we obtain the claim as desired.  $\square$

### 4.3 Finite sample guarantee

For the dual problem of SCOT (or COT), we also have a finite sample guarantee as follows. Denote  $J^* := \int_{\mathcal{X}} f(x)\mu(dx)$  as the expected value with the true  $\mu$ . Let  $\hat{J}_N(\varepsilon) := \sup_{\nu \in \mathcal{B}_\varepsilon \cap \mathcal{V}} \int_{\mathcal{Y}} f(y)\nu(dy)$  with  $\mathcal{B}_\varepsilon = \{\nu : \mathcal{W}_c(\hat{\mu}(\cdot|N, \varphi_N), \nu) \leq \varepsilon\}$ . With high probability,  $\hat{J}_N(\varepsilon)$  is an upper bound for  $J^*$  under certain conditions.

**Corollary 4.6.** *Suppose*

1.  $\mathcal{V}$  is large enough to include the true  $\mu$ ;
2. the cost  $c(x, y) = |x - y|_1$ ;
3. Assumption 4.1 holds;
4.  $\mu$  is Lipschitz in the sense of Backhoff-Veraguas et al. (2020, Assumption 1.4);

For a given level  $\delta_N \in (0, 1)$ , let  $\varepsilon_N := CN^{-1/(T+1)} + \left(\frac{1}{cN} \ln \left(\frac{2T}{\delta_N}\right)\right)^{1/2}$  with constants  $c$  and  $C$  from Backhoff-Veraguas et al. (2020, Theorem 1.7). Then

$$\mathbb{P}[J^* \leq \hat{J}_N(\varepsilon_N)] \geq 1 - \delta_N, \quad (4.16)$$

where  $\mathbb{P} := \mu^N$  is the product of  $N$  true measures. If  $\sum_{N=1}^{\infty} \delta_N < \infty$  and  $\lim_{N \rightarrow \infty} \varepsilon_N = 0$ , then any sequence  $\hat{\nu}_N$  satisfying  $\mathcal{W}_c(\hat{\mu}(\cdot|N, \varphi_N), \hat{\nu}_N) \leq \delta_N$ , converges under Wasserstein metric  $\mathcal{W}$  to  $\mu$  almost surely. Moreover,  $\hat{J}_N(\varepsilon_N) \downarrow J^*$  almost surely.

*Proof.* Denote  $\mathcal{AW}$  as the adapted Wasserstein distance in Backhoff-Veraguas et al. (2020). Since for any two measures, their  $\mathcal{AW} \geq \mathcal{W}_c \geq \mathcal{W}$ . If  $\mathbb{P}[\mathcal{AW}(\hat{\mu}(\cdot|N, \varphi_N), \mu) \geq \varepsilon_N] \leq \delta_N$ , then one has  $\mathbb{P}[\mathcal{W}_c(\hat{\mu}(\cdot|N, \varphi_N), \mu) \geq \varepsilon_N] \leq \delta_N$ . In other words, with probability at least  $1 - \delta_N$ , we have  $\mu \in \mathcal{B}_{\varepsilon_N}$ . Since  $\mu \in \mathcal{V}$  by assumption, we have  $J^* \leq \hat{J}_N(\varepsilon_N)$ . With constants  $c, C, \varepsilon$  in Backhoff-Veraguas et al. (2020, Theorem 1.7), we can set

$$\delta_N = 2T \exp(-cN\varepsilon^2), \quad CN^{-1/(T+1)} + \varepsilon = \varepsilon_N. \quad (4.17)$$

Canceling  $\varepsilon$ , we obtain the representation of  $\varepsilon_N$ . The remaining claim follows similarly as in Mohajerin Esfahani and Kuhn (2018, Theorem 3.6).  $\square$

### 4.4 Optimization algorithms

In this subsection, we further assume the objective  $f$  and the cost  $c(x, y)$  are differentiable. We first present the optimization algorithm for the dual problem of COT and OT. Consider the test function space  $\Gamma'$  with martingales since it is easier to implement.  $h_{l,t}$  and  $M_{l,t}$  are modeled by neural networks, with more details in the Appendix. To impose the martingale condition, Xu et al. (2020) penalizes  $M_{l,t}$  by the following term when it violates the martingale property:

$$p(M; \varphi_N) := \frac{1}{NT} \sum_{l=1}^L \sum_{t=1}^{T-1} \left| \sum_{n=1}^N \frac{M_{l,t+1}(\varphi_N(x_{1:t+1}^n)) - M_{l,t}(\varphi_N(x_{1:t}^n))}{\sqrt{\text{Var}[M_l]} + \eta} \right|,$$

where  $N$  is the sample size of  $\hat{\mu}$ ,  $\text{Var}[M_l]$  is the empirical variance of  $M_l$ , and  $\eta > 0$  is a small constant to avoid dividing by zero. In summary, the COT optimization problem is

$$\inf_{\lambda \geq 0, \gamma' \in \Gamma'} \lambda\varepsilon + \int_{y \in \mathcal{Y}} \sup \{f(y) - \lambda c(x, y) + \gamma'(x, y)\} \hat{\mu}(dx_{1:T}|N, \varphi_N) + \xi p(M; \varphi_N) \quad (4.18)$$

and  $\xi > 0$  is a weighting constant. We propose Algorithm 1 to evaluate inner maximization and outer minimization alternatively. Experimentally, multiple inner maximization steps yield more stable results, while the computational burden is higher.

---

**Algorithm 1**

---

- 1: **Input:** Objective  $f$ , network  $\gamma'(x, y)$ , initial  $\lambda > 0$
- 2: **for**  $O$  steps **do**
- 3:   Sample  $x$  (by simulation) and construct the adapted empirical measure
- 4:   **for**  $I$  steps **do**
- 5:     Maximize (4.18) over  $y$  with (stochastic) gradient descent and project  $y$  into  $\mathcal{Y}$
- 6:   **end for**
- 7:     Minimize (4.18) over  $\lambda$  and  $\gamma'$  and truncate parameters
- 8: **end for**
- 9: **Output:** network  $\gamma'$ ,  $y$ , constant  $\lambda$ , and dual value

---

For SCOT, suppose  $\nu \in \mathcal{V}$  is a parameterized model and we call it a generator of alternative measures. The exact computation of the Wasserstein distance is expensive. There are several optimization methods to approximate the Wasserstein distance  $\mathcal{W}(\hat{\mu}, \nu; \lambda, \gamma)$  in (3.7).

First, when  $\hat{\mu}$  and  $\nu$  are both discrete measures, Sinkhorn's algorithm is widely used (Genevay et al., 2016; Xu et al., 2020). For a transport plan  $\pi$ , denote the entropy as

$$S(\pi) = - \sum_{i,j} \pi_{ij} \log \pi_{ij}$$

for the discrete case with  $0 \log 0 = 0$  and

$$S(\pi) = - \int_{\mathcal{X} \times \mathcal{Y}} \ln \pi(dx, dy) \pi(dx, dy)$$

for the continuous case. The entropy regularized problem first considers the optimization over transport plans as

$$\inf_{\pi \in \Pi(\hat{\mu}, \nu)} \left\{ \int_{\mathcal{X} \times \mathcal{Y}} [-f(y) + \lambda c(x, y) - \gamma(x, y)] \pi(dx, dy) - \lambda \tau S(\pi) \right\}$$

with a parameter  $\tau > 0$ . Denote the corresponding minimizer as  $\pi^*(dx, dy; \tau)$ , which can be computed efficiently by Sinkhorn's algorithm. Define the regularized distance as

$$\mathcal{W}(\hat{\mu}, \nu; \lambda, \gamma, \tau) := \int_{\mathcal{X} \times \mathcal{Y}} [-f(y) + \lambda c(x, y) - \gamma(x, y)] \pi^*(dx, dy; \tau). \quad (4.19)$$

Finally, the entropy regularized SCOT optimization problem is

$$\sup_{\nu \in \mathcal{V}} \inf_{\lambda \geq 0, \gamma' \in \Gamma'} \lambda \varepsilon - \mathcal{W}(\hat{\mu}, \nu; \lambda, \gamma', \tau) + \xi p(M; \varphi_N). \quad (4.20)$$

Algorithm 2 presents the optimization method for the entropy regularized problem. We defer further implementation details to the Appendix.

If  $\nu$  is continuous and  $\hat{\mu}$  is discrete, Genevay et al. (2016) proposes an average SGD algorithm, which can be used to replace Sinkhorn's algorithm in the Algorithm 2.

Unfortunately, convergence analysis of general non-convex non-concave minimax optimization is open, while it has received great attention in recent years. Experimentally, the algorithms converge to some stationary points with properly chosen learning rates and initial values. In the next section, we consider numerical experiments and findings.

## 5 Numerical analysis

We consider two fundamental problems, volatility estimation and S&P 500 index prediction, from finance. Under specific objective and cost functions, we provide examples of encoding structural information into alternative measures modeling. Overall, the OT method ignores the temporal structure and exhibits more aggressive behaviors in out-of-sample testing. SCOT consistently performs better than COT and OT by exploiting the structural information.

---

**Algorithm 2**


---

- 1: **Input:** Objective  $f$ , network  $\gamma'(x, y)$ , generator  $\nu$ , initial  $\lambda > 0$
- 2: **for**  $I$  steps **do**
- 3:   Sample  $x$  (by simulation) and construct the adapted empirical measure
- 4:   Simulate sample  $y \sim \nu$  and construct the adapted empirical measure
- 5:   Calculate (4.19) with Sinkhorn's algorithm
- 6:   Minimize (4.20) over  $\lambda$  and  $\gamma'$  and truncate parameters
- 7:   Maximize (4.20) over  $\nu$  and truncate parameters
- 8: **end for**
- 9: **Output:** network  $\gamma'$ , generator  $\nu$ , constant  $\lambda$ , and dual value

---

### 5.1 Volatility estimation

The DM is concerned about the average value of volatility  $X$  over a discrete time period  $t = 1, \dots, T$ :

$$\frac{1}{T} \sum_{t=1}^T X_t. \quad (5.1)$$

The time interval is evenly spaced with a step size of  $dt$ . Suppose the volatility  $X_t$  takes values in the closed interval  $[x_{\min}, x_{\max}]$ .

For the structural information set  $\mathcal{V}$ , the DM uses the Jacobi model (Ackerer et al., 2018) that specifies the volatility process  $X_t$  as

$$dX_t = \kappa(\phi - X_t)dt + \sigma \sqrt{Q(X_t)}dW_t, \quad Q(x) = \frac{(x - x_{\min})(x_{\max} - x)}{(\sqrt{x_{\max}} - \sqrt{x_{\min}})^2},$$

with constant parameters  $\kappa > 0$ ,  $0 \leq x_{\min} < x_{\max}$ ,  $\phi \in (x_{\min}, x_{\max}]$ ,  $\sigma > 0$ , and initial state  $X_0 \in [x_{\min}, x_{\max}]$ .

In the simulation, we assume the true model is also a Jacobi model with parameters  $\kappa = 0.5$ ,  $\phi = 0.5$ ,  $\sigma = 0.2$ ,  $x_{\min} = 0.0$ ,  $x_{\max} = 1.0$ ,  $X_0 = 0.5$ . The DM can observe samples with length  $T = 20$  from the true model. Then the true mean (5.1) is close to 0.5.

To incorporate robustness, the DM considers distributionally robust estimation with OT, SOT, and SCOT. Consider a quadratic cost function  $c(x, y) = \sum_{t=1}^T (x_t - y_t)^2$ . We fix the radius as  $\varepsilon = 1.0$ . The OT solution is explicit and the robust value is around 0.72. For SOT and SCOT, we further suppose the DM believes the true model is a Jacobi model with unknown parameters. The DM embeds the structural information as follows. A Jacobi model with learnable parameters  $\kappa$ ,  $\phi$ , and  $\sigma$  is adopted to generate alternative scenarios. Moreover, the DM has prior beliefs on parameters. Especially, suppose the DM restricts the volatility-of-volatility  $\sigma$  into  $[0.1, 0.5]$ . The mean  $\phi$  is crucial in this problem. Denote the reference sample mean as  $\bar{x}^i = 1/T \sum_{t=1}^T x_t^i$ . The DM specifies the  $\phi$  in the alternative model as

$$\phi^i = \bar{x}^i + \phi_m.$$

$\phi_m$  can be interpreted as the mean missed by a specific sample. We use  $\phi^i$  as  $\phi$  and it is different for each sample path. We suppose the true  $x_{\min}$ ,  $x_{\max}$ ,  $X_0$ , and  $dt$  are known by the DM. Finally, the alternative sample is generated by

$$y_t^i = p\hat{x}_t^i + (1 - p)\bar{x}^i, \quad p \in [0, 1],$$

where  $\{\hat{x}_t^i\}_{t=1}^T$  is sampled from the alternative Jacobi model.  $p$  represents the probability that the DM trusts in the alternative sample. We fix  $p = 0.5$  in the default setting.

## Dual values and sample paths

Table 1 reports the dual values under various settings. We simulate the data semi-annually, monthly, weekly, and daily. The OT method has the highest mean near 0.723, which does not change when the step size  $dt$  varies. It agrees with the theoretical result since the worst case has a form as  $y_t = x_t + a$  for certain constant  $a$ . The SOT dual value is smaller than the OT counterpart, with a difference close to  $3 \sim 4\%$ . The reason is that SOT only samples from a proper alternative Jacobi model. SCOT further reduces the dual value by a difference near  $3 \sim 4\%$ . It is from the causality condition, which rules out some transport plans. The last column in Table 1 shows p-values from the Mann-Whitney U test. The alternative hypothesis is that the distribution of SOT dual value is stochastically greater than the SCOT counterpart. In all the cases, the p-values are small. We confirm that the SCOT dual values are smaller than the SOT ones. Figure (1a) shows mean values and confidence intervals for  $dt = 1/2$ . One can see the algorithms converge to significantly different outcomes.

$dt$	OT	SOT	SCOT	p-value
1/2	0.72314 (0.02704)	0.68202 (0.08201)	0.64809 (0.08525)	$5.8296 \times 10^{-9}$
1/12	0.72318 (0.02885)	0.67538 (0.08879)	0.64603 (0.09416)	$1.6060 \times 10^{-6}$
1/52	0.72313 (0.01724)	0.67889 (0.06433)	0.64415 (0.06933)	$1.4043 \times 10^{-8}$
1/252	0.72307 (0.00828)	0.69029 (0.03835)	0.65889 (0.04553)	$2.1613 \times 10^{-8}$

Table 1: Sample mean and standard deviation (in parentheses) of dual values. The time series length  $T = 20$ . The simulation runs for 3000 periods and is repeated by 50 instances. the last 200 values in each instance after convergence are used in the calculation.

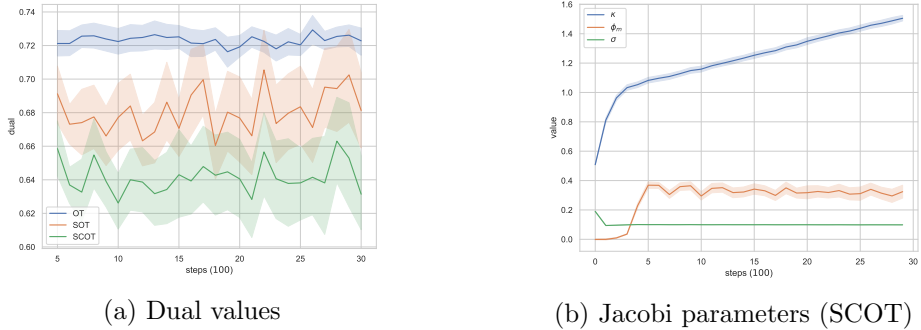


Figure 1: Average dual values and parameters across instances. Shadow areas are 95% confidence intervals and solid lines are mean values. Only  $dt = 1/2$  is presented for simplicity. Figure (1a) omits the periods before convergence and starts from the period 500 for better comparison.

Besides the difference in dual values, we also find the worst-case scenarios in SOT and SCOT depend on the choice of  $dt$ . When the step size is small, such as in days, the dual values are larger in both SOT and SCOT. A small step size makes the reference sample fluctuate in smaller regions. It is easier for the alternative Jacobi model to find more extreme scenarios. Indeed, Figure 2 illustrates the sample paths generated by different algorithms. Figure (2b) shows that the worst-case path  $y$  in OT is parallel to the reference  $x$ , irrelevant to the value of  $dt$ . However, it is not the case when comparing SOT and SCOT paths. When  $dt = 1/2$  and the  $x$  is volatile,  $y$  is also volatile. Instead, if  $dt$  is small and the path  $x$  is stable, the path  $y$  will grow almost linearly. Besides, SCOT and SOT generate closer paths when  $dt$  is small. Figure 2 indicates that SCOT and SOT learn very different temporal structures than the OT case. OT believes that the worst case is when volatility is shifted upward at every time point. SCOT and SOT think the worst case is when volatility rises rapidly with time.

To look deeper into SOT and SCOT, we consider the distribution of the difference in dual

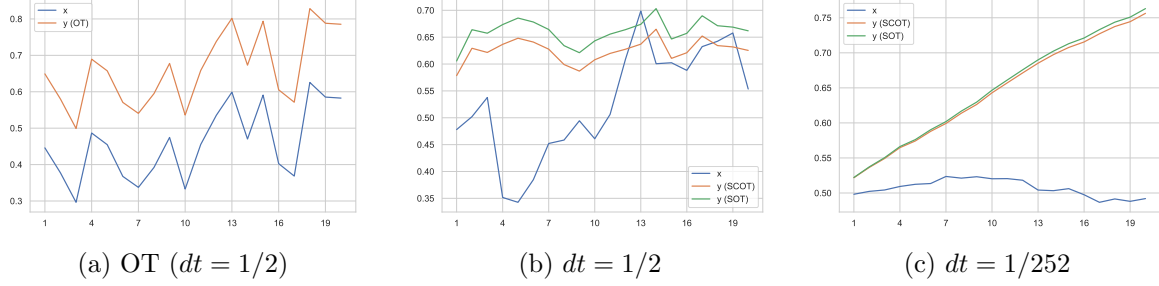


Figure 2: Sample paths under OT, SOT, and SCOT. Instances 0, 1, and 10 are used in these figures, respectively.

values across instances. Since SOT and SCOT outputs are in pairs, Figure 3 plots fifty sample differences by subtracting SCOT values from SOT ones, with samples from Table 1. A new phenomenon is that the distribution is bimodal, with one mode close to 0 and another close to 0.05. More precisely, Figure (3a) indicates that there are about 9 out of 50 instances that SCOT obtains a dual value equal to or even less than the SOT counterpart. In contrast, other instances locate mostly around  $0.04 \sim 0.05$ . There are very few instances with the difference between  $0.02 \sim 0.04$ . It is more prominent when we set  $dt = 1/252$ . Experimentally, if the neural network  $\gamma'(x, y)$  cannot find any punishment for violating causality, it sticks to zero. Otherwise, the penalty is close to a constant value. It is rare for the neural network to punish the violation smoothly, especially when  $dt$  is small.

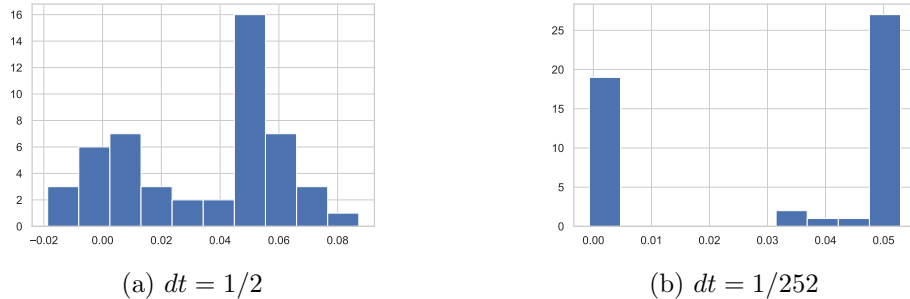


Figure 3: Bimodal phenomenon of the difference between dual mean values of SOT and SCOT.

## Parameters

	$dt$	1/2	1/12	1/52	1/252
SOT	$\kappa$	1.50477 (0.07761)	0.95344 (0.55625)	1.81585 (0.63885)	3.79290 (0.30512)
	$\phi_m$	0.32028 (0.15649)	0.37696 (0.40988)	0.93507 (0.47236)	2.48968 (0.30200)
	$\sigma$	0.09886 (0.00183)	0.10176 (0.00631)	0.10586 (0.01173)	0.11457 (0.02523)
SCOT	$\kappa$	1.50481 (0.07725)	0.94343 (0.54906)	1.81848 (0.63645)	3.79285 (0.30523)
	$\phi_m$	0.31611 (0.15578)	0.36761 (0.40435)	0.93754 (0.46999)	2.48966 (0.30188)
	$\sigma$	0.09890 (0.00188)	0.10159 (0.00571)	0.10585 (0.01212)	0.11454 (0.02506)

Table 2: Mean and standard deviations of  $\kappa$ ,  $\phi_m$ , and  $\sigma$  learned for the Jacobi model. The same simulation setting in Table 1 is adopted.

For the parameters in the alternative Jacobi model, Table 2 presents the mean and standard deviations of  $\kappa$ ,  $\phi_m$ , and  $\sigma$ . Figures 4 depicts an instance in SCOT to show some patterns that disappear after averaging over instances in Figure (1b). All parameters learned by SOT and SCOT are relatively close. There are three main observations. First,  $\sigma$  attains the lower bound

specified by the DM in all situations. It reflects that algorithms try to reduce fluctuations and use a deterministic  $y$  to depict the worst-case scenario. It is reasonable since one can find a constant larger than the reference sample mean  $\bar{x}^i$  to achieve the worst-case value. If we impose  $\sigma = 0$ , the learning progression is also easier, which is exactly the current algorithm with  $\sigma \geq 0.1$  trying to achieve. Second, Figure (4a) and (1b) show that the mean-reverting speed  $\kappa$  tends to reach a higher value. The algorithm wants to fix the path  $y^i$  close to  $\phi^i$ . When  $dt$  becomes smaller, Table 2 shows that  $\kappa$  becomes larger and the trend is stronger, consistent with the sample paths observed in Figure (2c). Third,  $\phi_m$ , the value missed by the sample mean  $\bar{x}^i$ , vibrates significantly, as shown in Figure (4b). It is closely related to the fluctuation in cost and  $\lambda$ , discussed later in Figure 6. This phenomenon reflects that the cost crosses the boundary of the (causal) Wasserstein ball repeatedly. When the cost is large and the alternative measure is out of the ball,  $\phi_m$  decreases to draw the measure back. The opposite case happens when  $\phi_m$  increases. Besides, Table 2 shows that  $\phi_m$  increases when  $dt$  decreases, resulting in a higher dual value. The difference in  $\phi_m$  for SOT and SCOT is bigger than other parameters when  $dt = 1/2$  and  $dt = 1/12$ . However, this difference is not the only source of the  $3 \sim 4\%$  gap in Table 1. The gap is also due to the penalty from  $\gamma'(x, y)$ .

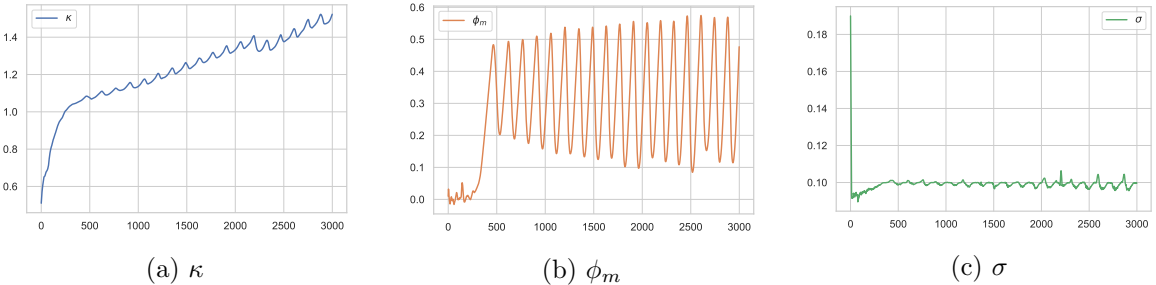


Figure 4: Parameters learned for the alternative Jacobi model. For simplicity, we choose the instance 10 in SCOT with  $dt = 1/2$ .

### Costs and $\lambda$

$dt$	OT	SOT	SCOT
1/2	1.00059 (0.14695)	0.92257 (0.53789)	0.91069 (0.53189)
1/12	1.00047 (0.14634)	0.83845 (0.58402)	0.80659 (0.57916)
1/52	1.00075 (0.14612)	0.76134 (0.45008)	0.76339 (0.44823)
1/252	1.00005 (0.14669)	0.86994 (0.32198)	0.86990 (0.32202)

Table 3: Mean and standard deviation of costs, with the same samples from Table 1.

$dt$	OT	SOT	SCOT
1/2	0.11295 (0.00442)	0.17388 (0.17494)	0.17405 (0.17348)
1/12	0.11255 (0.00330)	0.13884 (0.16094)	0.14015 (0.16260)
1/52	0.11207 (0.00126)	0.10645 (0.13989)	0.10708 (0.13962)
1/252	0.11240 (0.00329)	0.11133 (0.12604)	0.11135 (0.12610)

Table 4: Mean and standard deviation of  $\lambda$ . Samples are the same as in Table 1.

Recall that the radius is 1.0. Then we expect one of the following two conditions holds: (1) the cost  $\int_{\mathcal{X} \times \mathcal{Y}} c(x, y) \pi^*(dx, dy) = 1.0$  for the optimizer  $\pi^*$ ; or (2)  $\lambda^* = 0$  after convergence. Tables 3 and 4 summarize the statistics for the costs and the  $\lambda$  after convergence, respectively.

Overall, all algorithms have non-zero  $\lambda^*$ . From Table 3, one can observe that OT is stable with small variances. An instance in Figure 5 also confirms it. SOT and SCOT converge to costs close but slightly lower than 1.0 on average. Their variances are much higher than OT. Figure 6 reveals more details about convergence. Figure (6b) shows that the Lagrange multiplier  $\lambda$  reaches boundary zero and be reflected repeatedly. This behavior appears in SCOT and SOT across all the values of  $dt$ . It is related to the vibrating trajectories of  $\phi_m$  in Figure (4b). Since SOT also has this pattern, the vibration is from the structural design instead of training neural networks. On average, Table 4 documents that  $\lambda^*$  is positive for SOT and SCOT. Besides, when  $dt$  is small,  $\lambda^*$  under SOT and SCOT is also bigger than OT since the design of alternative models rules out some transport plans.

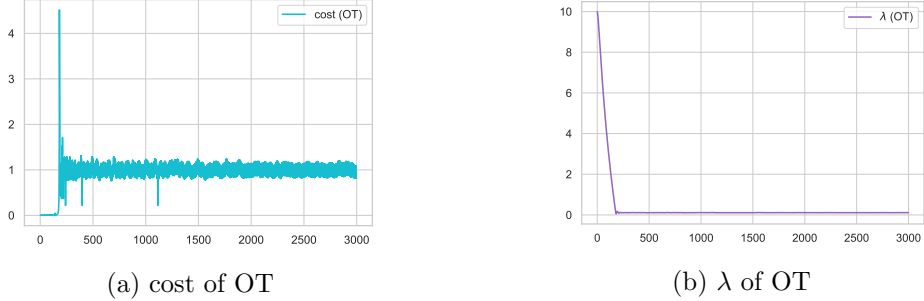


Figure 5: The evolution of the cost and  $\lambda$  under OT, with  $dt = 1/2$  and instance 0 for illustration.

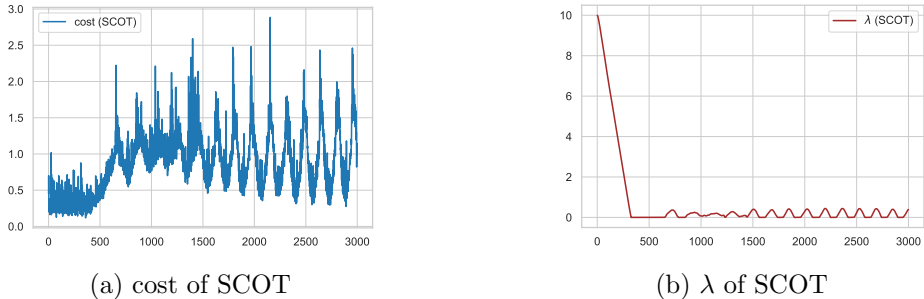


Figure 6: The evolution of the cost and  $\lambda$  under SCOT, with  $dt = 1/2$  and instance 0 for illustration.

## 5.2 S&P500 index prediction

For the empirical analysis, we consider a data set on S&P 500 from UCI machine learning repository <sup>1</sup>. We choose this data set since it is open source and results hereafter are publicly reproducible. It contains various daily features of the S&P 500 index, including momentum factors, technical indicators, oil and gold prices, and stock prices of major companies. Our problem of interest is, what is the highest index possible after certain trading days?

To accommodate this problem into our framework, we first need a function  $f$  such that  $\int_{\mathcal{X}} f(x_{1:T}) \hat{\mu}(dx) = r_{T+1}$ , where  $x_{1:T}$  is the current information available including past returns and  $r_{T+1}$  is the return of the index in the next period. This function  $f$  is not obvious. We propose to model  $f$  by a multilayer perceptron (MLP) neural network. First, we train the MLP  $f$  to predict the next return based on the current information  $x_{1:T}$ . Then, we fix the parameters of  $f$  and use it as the objective. Since the in-sample training may suffer from the over-learning issue and does not generalize very well, we consider the robust version as the supremum of  $\int_{\mathcal{Y}} f(y_{1:T}) \nu(dy)$  over a certain set of  $\nu$ .

<sup>1</sup>CNNpred: <https://archive.ics.uci.edu/ml/machine-learning-databases/00554/>

Crucially, the alternative measure  $\nu$  should be flexible and sophisticated enough to generate scenarios near the original distribution in the Wasserstein sense. We implement it as follows and refer to it as the generator  $\nu$  for  $y$ .

---

**Algorithm 3** Generator  $\nu$ 


---

- 1: **Input:** A sample path  $x$ . Noise variance  $\sigma^2 > 0$ . A neural network  $R$ .
- 2:  $x' \leftarrow x + z$  with random perturbation  $z \sim N(0, \sigma^2)$
- 3: Residual  $r \leftarrow R(x' - \text{mean}(x'))$
- 4:  $y \leftarrow x' + r$
- 5: **Output:**  $y$

---

Motivations behind Algorithm 3 are twofold. First, we inject random noises  $z$  to improve the robustness and regard  $x'$  as some alternative scenarios. Second, inspired by the residual networks (He et al., 2016), we combine  $x'$  with residual values  $r$  learned from the centralized  $x'$ , with the help from the network  $R$ . If the generator finds  $x'$  is complicated enough to represent the worst cases, then the network  $R$  will be zero. Otherwise,  $R$  will generate non-zero  $r$ . When the variance  $\sigma^2 = 0$  and the residual network  $R = 0$ , we recover the original empirical distribution. Before the generator  $\nu$  is adopted in the robust framework, we pre-train it to minimize the MSE loss between the distributions of  $y$  and  $x_{1:T}$ . Pre-training is on the parameters of  $R$  and can avoid  $\nu$  from being too far from the empirical distribution.

We apply the SOT and SCOT framework with the MLP objective  $f$  and the pre-trained generator  $\nu$ . Note that parameters of  $\nu$  are still learnable, while  $f$  is given. We train the generator with batches sampled from a given time horizon. An observation  $x_{1:T}$  also contains past returns in terms of the first index value of this observation. In SOT and SCOT, the generator aims to find the worst scenario judged by the multiplier  $\lambda$  and the function  $\gamma'(x, y)$  in SCOT. They act as the discriminators between alternative data  $y$  and observations  $x$ . For OT,  $y$  reduces to deterministic values with no generator. In all methods, we adopt the averaged quadratic cost function.

In-sample results for the non-robust benchmark, OT, COT, and SCOT, show that they can predict upper bounds for returns with an accuracy close to 100% after proper training. Thus, the out-of-sample test is more valuable to uncover their different capabilities. We apply the learned generator in the training phase to simulate the worst scenarios on test data, which are unseen before. Table 5 summarizes the statistics of the performance on several episodes, with 100 trading days per episode. For example, the first episode starts on the day of 2014/01/21 and includes 100 trading days. The mean value of returns during this episode is 1.719%. Note that returns are over 20 trading days and thus bigger in magnitude than daily returns. The benchmark uses the off-the-shelf  $f$  without incorporating robustness. It predicts upper bounds with a mean value of 2.5884%. 81 out of 100 predictions are higher than the real ones. The mean absolute error (MAE) of the benchmark prediction is 1.1515%. Overall, the non-robust benchmark can achieve an out-of-sample accuracy of 57.56% and an average MAE of 1.397% across all episodes considered, proving that  $f$  can serve as a benchmark model even without robustness.

Table 5 shows that robust methods SCOT, SOT, and OT predict higher mean values. As a result, they provide upper bounds more accurately. A comparison finds that OT has the highest mean values in most cases than others. However, if we compare SOT and SCOT with OT more carefully, we can observe that SCOT and SOT achieve a better trade-off between accuracy and errors represented by MAE and mean values. SCOT and SOT have the same average accuracy of 68.78%, with average MAEs of 1.5025% and 1.5077%, respectively. OT has an average accuracy of 72.33%, while the average MAE increases to 1.8665%. The increment on MAE is not proportional to that of the accuracy. Importantly, it is not due to extreme high returns in tails. Figure 8 uncovers that OT predictions sometimes move downward, that

is, underestimate high returns even than the benchmark. In some episodes, SCOT and SOT find more upper bounds correctly, while MAE is even lower than OT. In other cases, they can sacrifice acceptable accuracy on upper bounds for more reduction on MAE. When we further compare SCOT with SOT, SCOT is slightly, but consistently, better than SOT. SCOT has a lower mean and MAE, while the accuracy remains the same. Thus, we conclude that SCOT performs better than SOT. Considering the trade-off between accuracy and MAE, SCOT and SOT are better than OT.

Starting date	Statistics	Benchmark	SCOT	SOT	OT
2014-01-21	mean (real = 1.7190)	2.5884	2.8791	2.8899	3.4225
	prediction > real	81	89	89	95
	MAE	1.1515	1.3546	1.3631	1.8400
2014-06-13	mean (real = 0.8597)	0.9628	1.4868	1.4948	1.6017
	prediction > real	58	71	71	62
	MAE	1.1865	1.3870	1.3910	2.0529
2014-11-04	mean (real = 0.4437)	-0.5886	-0.1771	-0.1754	0.4851
	prediction > real	23	38	38	47
	MAE	1.4840	1.3163	1.3159	1.4840
2015-03-31	mean (real = -1.3928)	-0.4524	-0.1164	-0.0852	0.3281
	prediction > real	57	67	67	68
	MAE	1.7390	1.8110	1.8219	2.1626
2015-08-21	mean (real = -0.6780)	-1.4477	-1.0282	-1.0159	-0.1316
	prediction > real	40	46	46	50
	MAE	2.5014	2.4229	2.4227	2.8844
2016-01-14	mean (real = 1.9469)	2.1006	2.3748	2.4055	3.1296
	prediction > real	56	66	66	75
	MAE	1.1630	1.2247	1.2373	1.6572
2016-06-08	mean (real = 0.7071)	1.8116	2.3004	2.3050	2.5557
	prediction > real	87	94	94	94
	MAE	1.3528	1.7659	1.7698	1.9459
2016-10-28	mean (real = 1.7469)	1.5379	2.1868	2.1922	1.9043
	prediction > real	43	68	68	60
	MAE	0.8979	1.0115	1.0124	0.8932
2017-03-24	mean (real = 0.8811)	1.4044	1.6518	1.6637	2.7597
	prediction > real	73	80	80	100
	MAE	1.0974	1.2284	1.2352	1.8786

Table 5: Out-of-sample performance of four methods. The first column gives the starting date of every 100-trading-day test period. The first starting date is at the position of the 1000th row in the data frame and the last is at the 1800th. The benchmark method uses the target network  $f$  without robustness formulation. All numbers are in percentage.

Since SCOT is better than SOT, then we focus on SCOT and OT only. To develop a detailed understanding of them, Figures 7 and 8 present the time series for the second episode starting on the day of 2014/06/13. In Figure 7, the black empty circles represent the real target returns. The vertical dotted lines indicate the days when the non-robust benchmark predicts a higher return than the real ones. The benchmark usually gives correct upper bounds for low returns and misses certain high returns. The red vertical markers indicate the correct upper bounds by OT, while the blue horizontal markers show the correct SCOT upper bounds. For this episode, the difficulty is mainly in the last 30 trading days when returns rise significantly.

To reveal the sign and magnitude of predictions in contrast to true returns, Figure 8 calculates the difference between the predictions and returns. SCOT and OT values are close to the grey solid curve representing the benchmark. OT underestimates most of the last 30 returns, which is even more severe than the benchmark. SCOT estimates a little more values correctly during this last period. It consistently provides higher returns than the benchmark. Overall,

the main observation from Figure 8 is that OT overestimates and underestimates more severely when the benchmark shows the same issue. In other words, OT behaves more aggressively during extreme situations. Distinctly, SCOT has slightly higher predictions than the benchmark. We attribute this desired behavior to the structure of the generator  $\nu$  and the temporal condition imposed by the causality constraint. SCOT becomes more stable and consistent to find upper bounds for returns.

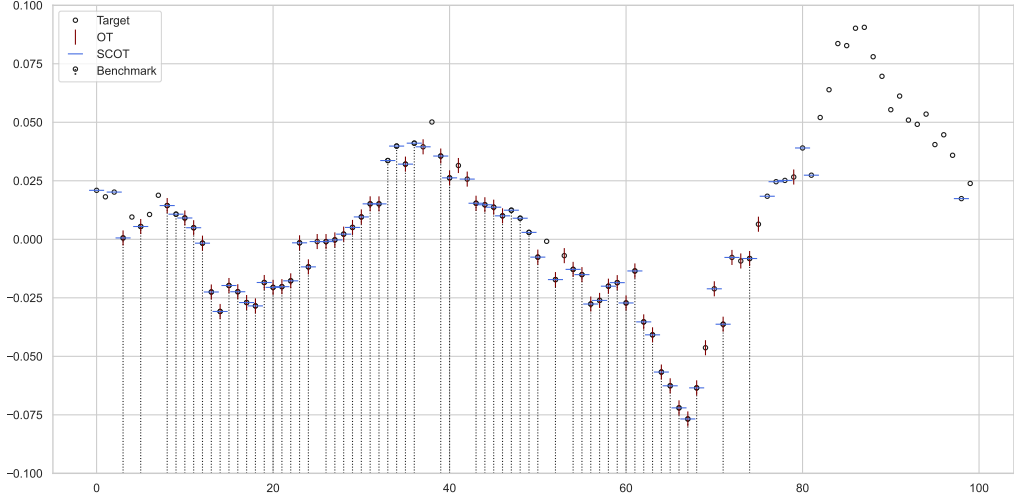


Figure 7: Returns and correct upper bound locations in the second episode of Table 5. Black circles represent true returns measured in 20 trading days. Dotted lines indicate the correct upper bounds by the non-robust benchmark. Red vertical markers and blue horizontal markers are for OT and SCOT, respectively. There are overlaps on correct upper bounds.

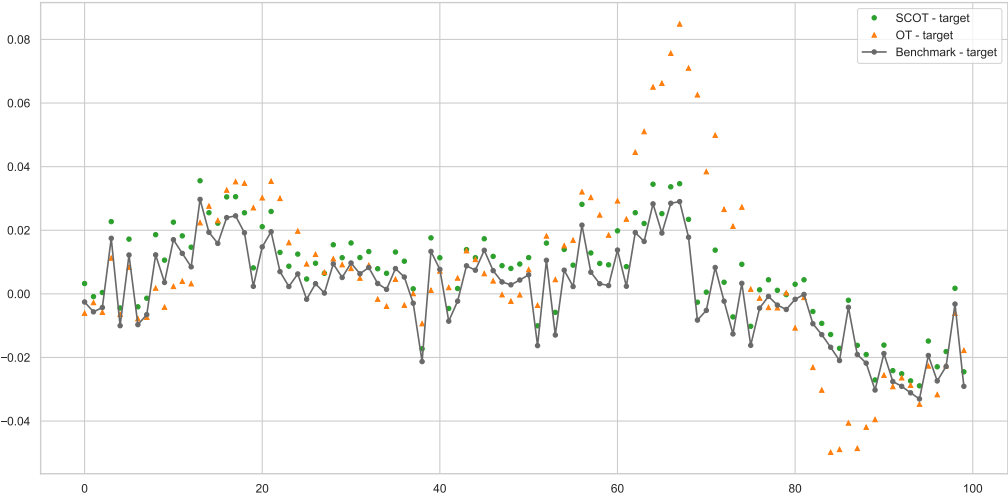


Figure 8: Difference between predictions and real returns in the second episode of Table 5. The grey solid curve shows benchmark predictions minus returns. Green dots and orange triangles are SCOT and OT predictions deducted by returns, respectively.

Although Figures 7 and 8 only present the second episode as an example, the observations summarized above are persistent in other episodes of Table 5. We can conclude that SCOT is an attractive alternative to the OT formulation.

## 6 Conclusions

This work considers causality constraint and structural information in distributionally robust risk evaluation. Several open questions are left. First, after approximation with neural networks, the dual problems of SCOT and COT belong to the general non-convex non-concave minimax optimization problem. Optimization errors and convergence analysis are less understood. Second, the DM may control the underlying processes and alter the uncertainty in distributions. It becomes interesting to consider such problems in the future.

## References

Acciaio, B., Backhoff-Veraguas, J., and Jia, J. (2021). Cournot–Nash equilibrium and optimal transport in a dynamic setting. *SIAM Journal on Control and Optimization*, 59(3), 2273–2300.

Acciaio, B., Backhoff-Veraguas, J., and Zalashko, A. (2020). Causal optimal transport and its links to enlargement of filtrations and continuous-time stochastic optimization. *Stochastic Processes and their Applications*, 130(5), 2918–2953.

Ackerer, D., Filipović, D., and Pulido, S. (2018). The Jacobi stochastic volatility model. *Finance and Stochastics*, 22(3), 667–700.

Backhoff-Veraguas, J., Bartl, D., Beiglböck, M., and Eder, M. (2020a). Adapted Wasserstein distances and stability in mathematical finance. *Finance and Stochastics*, 24(3), 601–632.

Backhoff-Veraguas, J., Bartl, D., Beiglböck, M., and Eder, M. (2020b). All adapted topologies are equal. *Probability Theory and Related Fields*, 178(3), 1125–1172.

Backhoff-Veraguas, J., Bartl, D., Beiglböck, M., and Wiesel, J. (2020). Estimating processes in adapted Wasserstein distance. *arXiv preprint arXiv:2002.07261*.

Backhoff-Veraguas, J., Beiglböck, M., Lin, Y., and Zalashko, A. (2017). Causal transport in discrete time and applications. *SIAM Journal on Optimization*, 27(4), 2528–2562.

Bartl, D., Drapeau, S., and Tangpi, L. (2020). Computational aspects of robust optimized certainty equivalents and option pricing. *Mathematical Finance*, 30(1), 287–309.

Ben-Tal, A., Bertsimas, D., and Brown, D. B. (2010). A soft robust model for optimization under ambiguity. *Operations Research*, 58(4-part-2), 1220–1234.

Bertsekas, D. P. and Shreve, S. E. (1996). *Stochastic optimal control: the discrete-time case*, volume 5. Athena Scientific.

Blanchet, J., Chen, L., and Zhou, X. Y. (2021). Distributionally robust mean-variance portfolio selection with Wasserstein distances. *Management Science*.

Blanchet, J. and Murthy, K. (2019). Quantifying distributional model risk via optimal transport. *Mathematics of Operations Research*, 44(2), 565–600.

Eckstein, S., Kupper, M., and Pohl, M. (2020). Robust risk aggregation with neural networks. *Mathematical Finance*, 30(4), 1229–1272.

Galichon, A. (2016). *Optimal transport methods in economics*. Princeton University Press.

Gao, R. and Kleywegt, A. J. (2016). Distributionally robust stochastic optimization with Wasserstein distance. *arXiv preprint arXiv:1604.02199*.

Genevay, A., Cuturi, M., Peyré, G., and Bach, F. (2016). Stochastic optimization for large-scale optimal transport. *Advances in Neural Information Processing Systems*, 29.

Golowich, N., Rakhlin, A., and Shamir, O. (2018). Size-independent sample complexity of neural networks. In *Conference On Learning Theory*, (pp. 297–299). PMLR.

Goodfellow, I., Bengio, Y., and Courville, A. (2016). *Deep learning*. MIT press.

Guo, G. and Obłój, J. (2019). Computational methods for martingale optimal transport problems. *The Annals of Applied Probability*, 29(6), 3311–3347.

Han, B., Pun, C. S., and Wong, H. Y. (2021). Robust state-dependent mean–variance portfolio selection: a closed-loop approach. *Finance and Stochastics*, 25(3), 529–561.

Hansen, L. and Sargent, T. J. (2001). Robust control and model uncertainty. *American Economic Review*, 91(2), 60–66.

Hansen, L. P. (2014). Nobel lecture: Uncertainty outside and inside economic models. *Journal of Political Economy*, 122(5), 945–987.

He, K., Zhang, X., Ren, S., and Sun, J. (2016). Deep residual learning for image recognition. In *Proceedings of the IEEE conference on computer vision and pattern recognition*, (pp. 770–778).

Hoseinzadeh, E. and Haratizadeh, S. (2019). CNNpred: CNN-based stock market prediction using a diverse set of variables. *Expert Systems with Applications*, 129, 273–285.

Ismail, A. and Pham, H. (2019). Robust Markowitz mean-variance portfolio selection under ambiguous covariance matrix. *Mathematical Finance*, 29(1), 174–207.

Knight, F. H. (1921). *Risk, uncertainty and profit*, volume 31. Houghton Mifflin.

Lassalle, R. (2013). Causal transference plans and their Monge-Kantorovich problems. *arXiv preprint arXiv:1303.6925*.

Maenhout, P. J. (2004). Robust portfolio rules and asset pricing. *Review of Financial Studies*, 17(4), 951–983.

Mohajerin Esfahani, P. and Kuhn, D. (2018). Data-driven distributionally robust optimization using the Wasserstein metric: Performance guarantees and tractable reformulations. *Mathematical Programming*, 171(1), 115–166.

Mohri, M., Rostamizadeh, A., and Talwalkar, A. (2018). *Foundations of Machine Learning*. MIT Press.

Peng, S. (2010). Nonlinear expectations and stochastic calculus under uncertainty. *arXiv preprint arXiv:1002.4546*.

Peyré, G., Cuturi, M., et al. (2019). Computational optimal transport: With applications to data science. *Foundations and Trends® in Machine Learning*, 11(5-6), 355–607.

Pflug, G. and Wozabal, D. (2007). Ambiguity in portfolio selection. *Quantitative Finance*, 7(4), 435–442.

Pflug, G. C. and Pichler, A. (2012). A distance for multistage stochastic optimization models. *SIAM Journal on Optimization*, 22(1), 1–23.

Pflug, G. C. and Pichler, A. (2016). From empirical observations to tree models for stochastic optimization: convergence properties. *SIAM Journal on Optimization*, 26(3), 1715–1740.

Reppen, A. M. and Soner, H. M. (2020). Bias-variance trade-off and overlearning in dynamic decision problems. *arXiv preprint arXiv:2011.09349*.

Santambrogio, F. (2015). Optimal transport for applied mathematicians. *Birkhäuser, NY*, 55(58-63), 94.

Uppal, R. and Wang, T. (2003). Model misspecification and underdiversification. *The Journal of Finance*, 58(6), 2465–2486.

Villani, C. (2009). *Optimal transport: old and new*, volume 338. Springer.

Wei, C. and Ma, T. (2019). Data-dependent sample complexity of deep neural networks via Lipschitz augmentation. *Advances in Neural Information Processing Systems*, 32.

Xu, T. and Acciaio, B. (2021). Quantized conditional COT-GAN for video prediction. *arXiv preprint arXiv:2106.05658*.

Xu, T., Li, W. K., Munn, M., and Acciaio, B. (2020). COT-GAN: Generating sequential data via causal optimal transport. *Advances in Neural Information Processing Systems*, 33, 8798–8809.

Zhou, Z., Blanchet, J., and Glynn, P. W. (2021). Distributionally robust martingale optimal transport. *arXiv preprint arXiv:2106.07191*.

## A Training details of the volatility estimation

Hyper-parameters and updates	Values
Common	
initial value of $\lambda$	10.0
batch size	4
number of iterations	3000
SOT and SCOT	
initial value of $\kappa$	0.5 (value of the true model)
initial value of $\phi_m$	0
initial value of $\sigma$	0.2 (value of the true model)
number of LSTMs in $h$ and $M$	2
hidden size of LSTM	4
learning rate of LSTMs in $h$ and $M$	0.05
learning rate of Jacobi model	0.01
velocity of momentum on updating $\lambda$	$v \leftarrow 0.9v - \nabla_\lambda / (0.1 \times \text{iter} + 200)$
truncation threshold of LSTM parameters	$[-5.0, 5.0]$
truncation threshold of $\sigma$	$[0.1, 0.5]$
entropy regularization	$\lambda\tau = 0.01\lambda + 10^{-5}$ for stability
martingale regularization	$\xi = 100.0$
martingale stability constant	$\eta = 10^{-6}$
OT	
initial value of $y$	$x + N(0, 0.001)$
updates of $y$	$y \leftarrow y + 50/(\text{iter} + 1) \times \nabla_y /  \nabla_y $
velocity of momentum on updating $\lambda$	$v \leftarrow 0.9v - \nabla_\lambda / (\text{iter} + 100)$

Table 6: Hyper-parameters and updating equations in OT, SOT, and SCOT. iter stands for the current number of iterations.  $\nabla_\lambda$  is the first-order derivative with respect to  $\lambda$ .

**Network architecture.** We implement the continuous bounded function  $h$  and martingale  $M$  by stacked LSTMs. LSTM is a variant of RNN with better empirical performance in many tasks.

Hyper-parameters and updates	Values
Common	
batch size	32
number of iterations	2000
radius $\varepsilon$	0.4
time steps in series	20
number of input features	16
number of output feature	1
initial value of $\lambda$	1.0
SOT and SCOT	
LSTM hidden size	4
MLP network hidden size	256 and 64
learning rate of objective $f$ optimizer	$5 \times 10^{-3}$
learning rate of generator optimizer	$10^{-4}$
learning rate of $M$ and $h$ net	$5 \times 10^{-4}$
learning rate of generator $y$ net	$5 \times 10^{-6}$
random noise on $x$ (in-sample phase)	$N(0, 10^{-2})$
random noise on $x$ (out-of-sample phase)	$N(0, 10^{-3})$
velocity on updating $\lambda$ in SOT and SCOT	$v \leftarrow 0.9v - \nabla_\lambda / (0.1 \times \text{iter} + 200)$
truncation threshold of $M$ parameters	$[-0.5, 0.5]$
truncation threshold of $h$ parameters	$[-1.0, 1.0]$
OT	
initial value of $y$	$x + N(0, 10^{-3})$
updates of $y$	$y \leftarrow y + 20 / (\text{iter} + 1) \times \nabla_y /  \nabla_y $
velocity on updating $\lambda$ in OT	$v \leftarrow 0.9v - \nabla_\lambda / (\text{iter} + 100)$

Table 7: Hyper-parameters in S&P 500 prediction. We adopt the same setting in Table 6 for parameters related to Sinkhorn’s algorithm.

To incorporate boundedness, we clamp parameters of LSTMs into certain bounded intervals, listed in Table 6. Initialize LSTM parameters with default methods in PyTorch.

**Optimization.** For LSTM, we use the Adam optimizer with learning rates in Table 6. For the optimization on  $\lambda$ , we implement SGD with momentum, see e.g. Goodfellow et al. (2016, Algorithm 8.2). The velocity updates are listed in Table 6. Truncate  $\lambda$  to be non-negative. For updating  $y$  in OT, we use SGD.  $y$  is usually high-dimensional even under small batches. Experimentally, we obtain more stable convergence when normalizing the gradient by its  $l_1$  norm. The stopping criterion of inner maximization is when relative changes in the objective are sufficiently small. The initial value of  $y$  is  $x$  perturbed by random noise. The initial value of  $\lambda$  is a sufficiently large positive constant.

## B Training details of S&P 500 prediction

**Data pre-processing.** We select 16 features from the original data set, including ‘Close’, ‘Volume’, ‘mom1’, ‘mom3’, ‘ROC\_15’, ‘EMA\_20’, ‘Oil’, ‘Gold’, ‘DAAA’, ‘AAPL’, ‘JNJ’, ‘XOM’, ‘TE1’, ‘DE1’, ‘S&P-F’, and ‘Dollar index-F’. Descriptions of these features are available in Hoseinzade and Haratizadeh (2019, Appendix I). We start from observations without missing data. We further scale several features to maintain similar magnitudes. The returns of S&P 500 are measured in terms of the starting point.

**Network architecture.** The residual network  $R$  is also modeled by LSTMs stacked together. The bounds of the parameters are in Table 7. The objective  $f$  is an MLP with Leaky ReLU activation functions. Initialize all their parameters with default methods in PyTorch.

**Optimization.** For MLP, we also use the Adam optimizer with learning rates in Table 7. The velocity update of  $\lambda$  is in Table 7.